https://doi.org/10.1016/j.bioorg.2024.107587

Bioorganic Chemistry

Synthesis and Pharmacological Evaluation of Novel N-aryl-cinnamoyl-hydrazone Hybrids Designed as Neuroprotective Agents for the Treatment of Parkinson's Disease

--Manuscript Draft--

Manuscript Number:	BIOORG-D-24-00951
Article Type:	Full Length Article
Keywords:	Parkinson's disease; cinnamic acid hybrids; N-aryl-cinnamoyl-hydrazones; molecular hybridization; neurodegenerative diseases
Corresponding Author:	Claudio Viegas Jr Federal University of Alfenas BRAZIL
First Author:	Matheus de Freitas Silva
Order of Authors:	Matheus de Freitas Silva
	Cindy Juliet Cristancho Ortiz, PhD
	Letícia Ferreira Coelho, bachelor
	Letizia Pruccoli, PhD
	Leonardo Pisani, PhD
	Marco Catto, PhD
	Giulio Poli, PhD
	Tiziano Tuccinardi
	Fabiana Cardoso Vilela
	Alexandre Giusti-Paiva, PhD
	Marina Amaral Alves, PhD
	Hygor M. Ribeiro de Souza, bachelor
	Andrea Tarozzi, PhD
	Vanessa Silva Gontijo, PhD
	Claudio Viegas Jr
Abstract:	Molecular hybridization between structural fragments from the structures of curcumin (1) and resveratrol (2) was used as a designing tool to generate a new N-acyl-cinnamoyl-hydrazone hybrid molecular architecture. Twenty-eight new compounds were synthesized and evaluated for multifunctional activities related to Parkinson's disease (PD), including neuroprotection, antioxidant, metal chelating ability, and Nrf2 activation. Compounds 3b (PQM-161) and 3e (PQM-164) were highlighted for their significant antioxidant profile, acting directly as induced free radical stabilizers by DPPH and indirectly by modulating intracellular inhibition of t-BOOH-induced ROS formation in neuronal cells. The mechanism of action was determined as a result of Nrf2 activation by both compounds and confirmed by different experiments. Furthermore, compound 3e (PQM-164) exhibited a significant effect on the accumulation of α-synuclein and anti-inflammatory activity, leading to an expressive decrease in gene expression of iNOS, IL-1β, and TNF-α. Overall, these results highlighted compound 3e as a promising and innovative multifunctional drug prototype candidate for PD treatment.
Suggested Reviewers:	Maria Emilia Sousa, PhD University of Porto esousa@ff.up.pt Med Chem expertise
	Patrícia Dias Fernandes, PhD Federal University of Rio de Janeiro

	patricia.dias.icbufrj@gmail.com Pharmacologist
	Angela Russell, PhD Oxford University angela.russell@chem.ox.ac.uk Med Chem expert
	Giulia Sita, PhD Alma Mater Studiorum Universita di Bologna giulia.sita2@unibo.it neuropharmacologist
	Luiz Antônio Soares Romeiro, PhD University of Brasilia lasromeiro@gmail.com Med Chem expert
Opposed Reviewers:	

Cover Letter

MINISTÉRIO DA EDUCAÇÃO
Universidade Federal de Alfenas . UNIFAL-MG
Rua Gabriel Monteiro da Silva, 714 . Alfenas/MG . CEP 37130-000
Fone: (35) 3299-1000 . Fax: (35) 3299-1063

Laboratório de Pesquisa em Química Medicinal
Laboratory of Research in Medicinal Chemistry

Alfenas, April 3rd, 2024.

To Professor Mark D. Distefano
Editor-in-Chief
Bioorganic Chemistry Journal

Dear Prof. Distefano,

I have the pleasure of sending you the manuscript entitled "Synthesis, and Pharmacological Evaluation of Novel *N*-aryl-cinnamoyl-hydrazone Hybrids Designed as Neuroprotective Agents for the Treatment of Parkinson's Disease", which I hope could be considered for publication in Bioorganic Chemistry.

In this paper, we describe the synthesis and pharmacological evaluation of a new series of *N*-aryl-cinnamoyl-hydrazone hybrid compounds with remarkable multifunctional properties and a simple and innovative structural architecture. Two of these compounds showed significant antioxidant, neuroprotective, and anti-neuroinflammatory properties, without cyto- and neurotoxicity, and good predicted druggability properties.

Thanks in advance for your attention, and I hope that this manuscript could be suitable for publication in Bioorganic Chemistry.

Sincerely Yours,

Prof. Claudio Viegas Jr.
PeQuiM, Institute of Chemistry, UNIFAL-MG
cvjviegas@gmail.com

HIGHLIGHTS

- Novel series of *N*-aryl-cinnamoyl-hydrazone was designed as curcumin-resveratrol multifunctional hybrids for PD.
- Compounds **3b (PQM-161)** and **3e (PQM-164)** exhibited expressive direct antioxidant activity on DPPH and neuronal-induced oxidative stress conditions.
- Compound **3e (PQM-164)** showed significant anti-inflammatory activity against 6-OHDA-induced neuronal damage, inhibiting the gene expression of IL-1β, iNOS and TNFα from activated microglial cells.
- **3e (PQM-164)** exhibited a significant effect on the accumulation of α-synuclein, promoting protein clearance.
- Compounds **3b (PQM-161)** and **3e (PQM-164)** showed good *in silico* predicted ADME parameters and no significant toxicity.
- Compound **3e (PQM-164)** seems to be a promising drug candidate prototype for the development of genuine multifunctional drugs for Parkinson's disease.

Synthesis and Pharmacological Evaluation of Novel *N*-aryl-cinnamoyl-hydrazone Hybrids Designed as Neuroprotective Agents for the Treatment of Parkinson's Disease

Matheus de Freitas Silva[1,2], Cindy Juliet Cristancho Ortiz[1], Letícia Ferreira Coelho[1], Letizia Pruccoli[2], Leonardo Pisani[3], Marco Catto[3], Giulio Poli[4], Tiziano Tuccinardi[4], Fabiana Cardoso Vilela[5], Alexandre Giusti-Paiva[6], Marina Amaral Alves[7], Hygor M. Ribeiro de Souza[7], Andrea Tarozzi[2], Vanessa Silva Gontijo[1], and Claudio Viegas Jr.[1]*

[1] PeQuiM-Laboratory of Research in Medicinal Chemistry, Federal University of Alfenas, Jovino Fernandes Sales Avenue 2600, 37133-840 Alfenas, Brazil
[2] Department for Life Quality Studies, Alma Mater Studiorum-University of Bologna, Corso d'Augusto 237, 47921 Rimini, Italy
[3] Department of Pharmacy-Pharmaceutical Sciences, University Aldo Moro of Bari, Via E. Orabona 4, 70125 Bari, Italy
[4] Department of Pharmacy, University of Pisa, Via Bonanno 33, 56126 Pisa, Italy
[5] Center of Innovation and Pre-clinical Assays- CIEnP, 88056-000 Florianopolis, Brazil
[6] Department of Physiological Sciences, Center of Biological Sciences, Federal University of Santa Catarina, 88040-900 Florianopolis, Brazil
[7] LabMeta, Metabolomics Laboratory, Institute of Chemistry, Federal University of Rio de Janeiro, 21941-598 Rio de Janeiro, Brazil

*Corresponding author: Claudio Viegas Jr., Institute of Chemistry, Laboratory of Research on Medicinal Chemistry, Jovino Fernandes Sales Ave. 2600, Room E106A. Federal University of Alfenas. 37133-840 Alfenas-MG, Brazil. Tel +55 (35) 3701-1880. e-mail: cvjviegas@gmail.com

ABSTRACT

Molecular hybridization between structural fragments from the structures of curcumin (**1**) and resveratrol (**2**) was used as a designing tool to generate a new *N*-acyl-cinnamoyl-hydrazone hybrid molecular architecture. Twenty-eight new compounds were synthesized and evaluated for multifunctional activities related to Parkinson's disease (PD), including neuroprotection, antioxidant, metal chelating ability, and Nrf2 activation. Compounds **3b (PQM-161)** and **3e (PQM-164)** were highlighted for their significant antioxidant profile, acting directly as induced free radical stabilizers by DPPH and indirectly by modulating intracellular inhibition of *t*-BOOH-induced ROS formation in neuronal cells. The mechanism of action was determined as a result of Nrf2 activation by both compounds and confirmed by different experiments. Furthermore, compound **3e (PQM-164)** exhibited a significant effect on the accumulation of α-synuclein and anti-inflammatory activity, leading to an expressive decrease in gene expression of iNOS, IL-1β, and TNF-α. Overall, these results highlighted compound **3e** as a promising and innovative multifunctional drug prototype candidate for PD treatment.

KEYWORDS: Parkinson's disease; cinnamic acid hybrids; *N*-aryl-cinnamoyl-hydrazones; molecular hybridization; neurodegenerative diseases.

1. Introduction

Parkinson's disease (PD) is the second most multifactorial neurodegenerative disease (ND), after Alzheimer's disease, associated with significant motor and behavioral disability and decreased quality of life[1,2]. The major neuropathological hallmarks of PD are the loss of dopaminergic neurons in the substantia nigra, which causes striatal dopamine deficiency, and intracellular inclusions containing aggregates of α-synuclein, also known as Lewy bodies[3]. The underlying molecular pathogenesis involves changes in multiple pathways and mechanisms such as oxidative stress (OS), altered Ca^{2+} homeostasis and axonal transport, mitochondrial dysfunction, and α-synuclein misfolding [3]. In this context, there is growing evidence that glial cells, including microglia and astrocytes, likely contribute to the PD's pathogenesis by both the loss of their normal homeostatic functions and the activation of neuroinflammation by the release of proinflammatory cytokines [4].

Among the pathogenic events, OS plays an important role in the degeneration of dopaminergic neurons during the progression of the disease [5]. In particular, there are different sources of increased OS in PD, such as dopamine auto-oxidation, mitochondrial dysfunction, increased free iron levels, and neuroinflammation that can lead to and reinforce neuronal dysfunction and death [6]. In this regard, enzyme monoamine oxidase B (MAO-B) can strengthen the OS by catalyzing the oxidative metabolism of dopamine with the formation of hydrogen peroxide (H_2O_2), which participates in Fenton-type reactions with Fe^{2+} to generate reactive oxygen species (ROS). Recent studies showed that isoform MAO-A can also play a role in dopamine metabolism, mostly in rodents and, to a lesser extent, in human basal ganglia, including the striatum [7]. Thus, both the high levels of ROS and the dyshomeostasis of Fe^{3+}/Fe^{2+} also promote the formation of α-synuclein misfolding and inclusions, amplifying the vicious cycle of OS at the neuronal level [6].

Generally, the brain is particularly vulnerable to oxidative damage due to the presence of high concentrations of oxygen, redox metals, and membrane polyunsaturated fatty acids [8]. In this regard, the activation of nuclear factor erythroid 2-related factor 2 (Nrf2) plays important roles in NDs such as increased production and release of glutathione (GSH), a powerful antioxidant and important defense agent in the PD treatment, as well as the inhibition of kinase glycogen synthase-3β (GSK-3β), which is an enzyme responsible for the modulation of programmed neuronal death [9,10].

The Nrf2-ARE (antioxidant-responsive element) antioxidant pathway has been widely studied as a therapeutic target, and its activation leads to very expressive antioxidant results [9,11–13]. At the cytoplasmic level, Nrf2 is bound to a protein called Kelch-like ECH-associated protein 1 (Keap1), which acts as a Nrf2 suppressor, and the complex Keap1/Nrf2 is the Nrf2 inactive form. Once activated

by phosphorylation, Nrf2 dissociates from Keap1 and is translocated to the cell nucleus, where it is recognized by the ARE, a DNA-specific region, triggering the genetic expression of detoxified, antioxidant (e.g. glutathione), and anti-inflammatory proteins [12,14].

In PD pathophysiology, it is observed a massive neuronal loss in the substantia nigra (SN) of the brain, causing a decrease in dopamine levels, and in turn, affecting motor and psychological abilities [15–18]. The MAO-B, along with presynaptic dopamine uptake, is the major dopamine-lowering pathway in the synaptic cleft since MAO-B plays the role of depleting the remaining synaptic dopamine. For this reason, MAO-B inhibition results in a significant increase in dopamine concentration and possibly assists in dopaminergic deficit in PD [19].

The current treatment of PD is based on the modulation of dopaminergic targets, such as the use of L-dopa, a drug that acts by increasing dopamine levels in the synaptic clefts within the CNS, and non-dopaminergic targets, such as rasagiline, an irreversible second-generation inhibitor of MAO-B, usually used in association with L-dopa [19]. However, long-term use of L-dopa may lead to serious side effects such as psychosis, dependence, and some cognitive effects [20,21].

In this context, nature is a rich source of an impressive diversity of chemical classes of bioactive molecules capable of modulating several aspects related to OS control, such as curcumin (**1**) and resveratrol (**2**), two widely known phenolic natural products (NPs) with prominent antioxidant, anti-inflammatory and neuroprotective properties [14,22,23]. Based on this range of biological activities, NPs have been widely used as sources of starting materials for semi-synthesis, drugs, active extracts, or structural models/molecular scaffolds used as inspiration for the design and synthesis of new neuroprotective drug candidate prototypes [24–27]. In this context, molecular hybridization (MH) has been explored as the most used tool for molecular design through the combination of diverse pharmacophore subunits from known different bioactive molecules to produce a single structural architecture with potentially improved pharmacological profile related to the parent compounds. In this way, MH aims to generate innovative and chemically diverse structural patterns that could result in improved biologically active compounds, representing innovation in drug discovery [28–30].

In this context, this work aimed to synthesize and evaluate a series of *N*-aryl-cinnamoyl-hydrazone hybrid compounds (**3** and **4**, Figure 1) designed by MH of curcumin (**1**) and resveratrol (**2**) as novel multitarget directed ligands capable to act as neuroprotective, antioxidant, metal chelators, and Nrf2 activators. As a result, 28 compounds were synthesized and submitted to a set of in vitro pharmacological experiments addressed to identify multiple properties related to direct and indirect antioxidant activity, inhibition of MAO-A/B and 6-hydroxydopamine (6-OHDA)-induced neuronal damage, and Nrf2 activation.

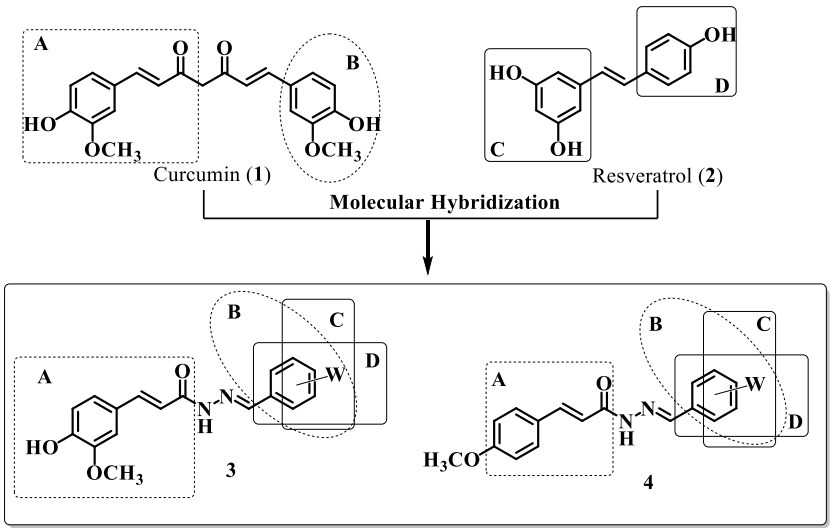

Figure 1. Molecular hybridization of curcumin (**1**) and resveratrol (**2**) in the design of the new series *N*-aryl-cinnamoyl-hydrazone derivatives **3** and **4**.

2. Results and discussion

2.1.Synthetic chemistry

The series of *N*-aryl-cinnamoyl-hydrazone derivatives **3a-w** and **4a-e** were synthesized as shown in *Scheme 1*, in a sequential two-step procedure. First, commercial ferulic cinnamic acid (**5a**) or 4-methoxy-cinnamic acid (**5b**) were converted to the correspondent hydrazides **6a** or **6b** by treatment with HOBT/EDAC and hydrazine monohydrate in ACN. Subsequently, intermediates **6a** or **6b** were subjected to an acid-catalyzed coupling reaction with a series of substituted aldehydes **7** to furnish the *N*-acylhydrazone derivatives **3a-w** and **4a-e**, in 22-85% overall yields. All compounds were characterized by IR,^{13}C, and ^{1}H NMR and HRMS techniques.

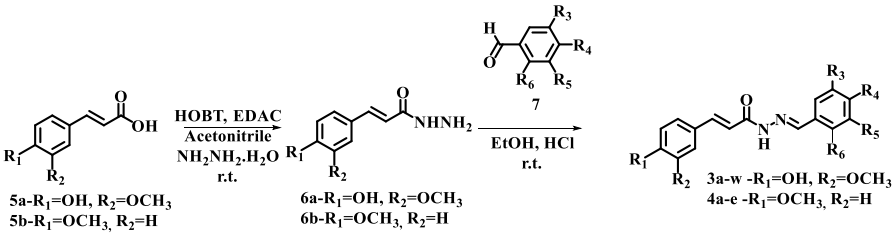

3a: R_3= R_5=R_6= H, R_4= OH
3b: R_3= R_5= OH, R_4= R_6= H
3c: R_3=R_5=R_6= H, R_4= OCH_3
3d: R_3=R_5= OCH_3, R_4= R_6= H
3e: R_3= R_6= H, R_4= OH, R_5= OCH_3
3f: R_3=R_5=R_6= H, R_4= F
3g: R_3=R_4=R_6 H, R_5= F
3h- R_3=R_4=R_5= H, R_6= F
3i- R_3=R_5=R_6= H, R_4=Cl
3j- R_3=R_4=R_6, R_5=Cl
3k- R_3=R_4=R_5= H, R_6= Cl
3l- R_3=R_5=R_6= H, R_4=Br
3m- R_3=R_5=R_6= H, R_4= $C(CH_3)_3$
3n- R_3=R_5=R_6= H, R_4= $N(CH_3)_2$
3o: R_3=R_5=R_6= H, R_4= $N(Et)_2$
3p: R_3=R_4=R_5= OCH_3, R_6= H
3q: R_3=R_4= OCH_3, R_5=R_6= H
3r: R_3=R_5=R_6= H, R_4= N-piperidine
3s: R_3=R_5=R_6= H, R_4= N-pyrrolidine
3t- R_3=R_5=R_6= H, R_4=N-morpholine
3u- R_3=R_5=R_6= H, R_4= N-imidazole
3v- R_3=R_5=R_6= H, R_4=3,5-pyrimidine
3w- R_3=R_4= H, R_5=R_6= 1,3-dioxole
4a- R_3=R_5=R_6= H, R_4= OH
4b- R_3=R_5= OH, R_4=R_6= H
4c- R_3=R_5=R_6= H, R_4= OCH_3
4d- R_3=R_5= OCH_3, R_4=R_6= H
4e- R_3=R_6= H, R_4=OH, R_5=OCH

Scheme 1. Synthetic route for *N*-aryl-cinnamoyl hydrazones **3a-w** and **4a-e**.

It is interesting to note that it was observed some duplicate ^{1}H NMR spectrum signals as well as unmatched integrals for the purely correspondent molecule, which was due to a possible geometric

stereoisomerism in the *N*-acylhydrazone spacer subunit. However, the HN-N bond of the *N*-acylhydrazone group also exhibits free rotation and may form a balance between antiperiplanar and syn-periplanar rotamers in solution. The formation of rotamers in *N*-acylhydrazone cinnamic derivatives have been previously described by Carvalho and co-workers [31], suggesting that the duplicate signals observed in some spectra of our final compounds were related to the presence of rotamers and not isomers. Palla and co-workers performed a detailed study on the conformational behavior of *N*-acyl-hydrazones, and the N-H bond signal was described at a chemical shift that may range from δ 10.67-10.43 for *E* isomers or δ 14.40-14.02 for *Z* isomers, depending on the preferred rotamer formed [32]. In the ^{1}H NMR spectrum of compound **3e,** the N-H bond showed chemical shifts at δ 11.35 and 11.16 (two rotamers) and, with no additional signal at δ 14.0 region, suggesting the presence of the single *E* isomer. In addition, the hydrazone C-H (N=C-H) bond has been usually described at δ 8.23-8.07 for the *E* isomer and at δ 7.12 for the *Z* isomer [32]. Accordingly, in the ^{1}H NMR spectrum of **3e,** the N=C-H bond was observed at δ 8.13 and 7.95, confirming the presence of the *E* isomer as a single product.

To confirm that **3e** occurs as a mixture of rotamers, sequential ^{1}H NMR spectra were obtained at different temperatures (27, 37, 47, 57, and 67°C). In Figure 2, it is possible to observe two pairs of simplets related to the N-H and C-H hydrogens of the hydrazone portion. The increase in temperature led to a progressive coalescence of each signal pair until 67ºC, registered as two simplets at δ 11.06 and δ 8.08 corresponding to the N-H and C-H, respectively. This result confirmed the presence of two rotamers, presumably attributed to the syn-periplanar conformer (sp, less stable) that, as the temperature rises, is converted into the antiperiplanar (ap, more stable) conformer, which is the thermodynamically most favorable conformation.

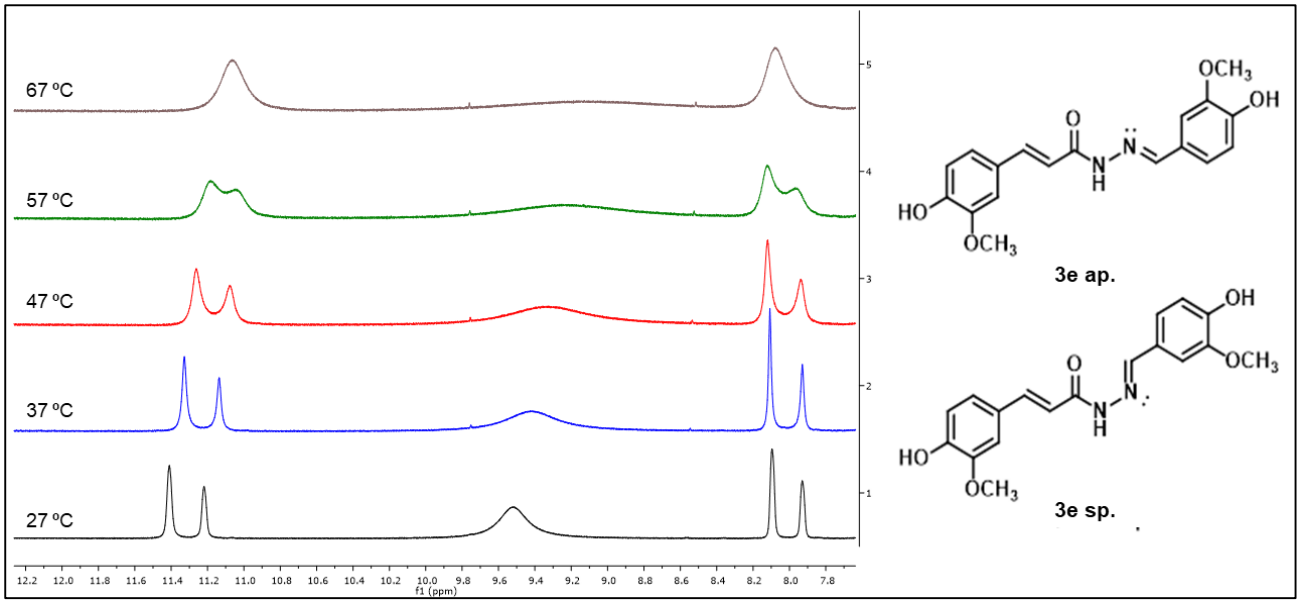

Figure 2. ^{1}H-NMR spectrum of 2-*N*-(4-hydroxy-3-methoxybenzyl)-3-(4-hydroxy-3-methoxyphenyl) acrylhydrazide (**3e**) at different temperatures (300 MHz, DMSO-d_6), and chemical structures of its anti-periplanar (**3e ap**) and syn-periplanar (**3e sp**) conformers.

2.2.Neurotoxicity and ADME properties

The neurotoxicity effects of all synthetic compounds were evaluated at different concentrations (2.5 - 80 µM) in human neuronal cells (SH-SY5Y) after 24 h of treatment by 3-(4,5-dimethylthiazol-2-yl)-2,5-diphenyl) tetrazole bromide (MTT) assay [33]. As presented in Table 1, compounds **3i-m**, **3p**, **3s**, **3w**, **4a,** and **4d** exhibited significant neuronal toxicity (IC_{50} values ranging from 4.94 to 48.43 µM), while the other compounds did not show neurotoxic effects at the highest concentration used (80 µM). The absence of cytotoxicity of compounds **3a-h**, **3n-o**, **3q-r**, **3t-v**, **4b-c,** and **4e** was further confirmed in renal VERO cell line, a suitable model to study the toxicity of new drugs, by MTT assay [34,35].

In parallel, in silico evaluation of ADME parameters of all hybrid compounds was performed by using the QikProp tool from Maestro (Schrödinger Release 2018-4, Schrödinger, LLC, New York, NY, USA, 2018). Computational data suggested no toxic effects for the target compounds at the neuronal level, also showing adequate oral absorption and BBB permeability, without violation of Lipinski's rule of five (Table 1), suggesting adequate druggability for the selected compounds **3a–h**, **3n–o**, **3q–r**, **3t-v**, **4b–c**, and **4e** for further antioxidant and neuroprotection investigation.

Table 1. Neurotoxicity and in silico ADME properties of the *N*-aryl-cinnamoyl-hydrazone derivatives **3a-w** and **4a-e**

Compound	Neurotoxicity	ADME[b]							
	IC_{50} (μM)[a]	MW	QP logPo/w	HBA	HBD	% HOA	QPPCaco	QPlogBB	QPlogHERG
3a (PQM-160)	>80	312.32	2.43	4.75	3	83.12	221.48	-1.77	-6,109
3b(PQM-161)	>80	328.32	2.26	5.50	4	72.93	67.74	-2.41	-5,973
3c (PQM-162)	>80	326.35	3.23	4.75	2	100.00	724.03	-1.21	-6,035
3d (PQM-163)	>80	356.38	3.28	5.50	2	100.00	769.67	-1.25	-5,784
3e (PQM-164)	>80	342.35	2.53	5.50	3	84.72	250.53	-1.77	-5,861
3f (PQM-211)	>80	314.32	3.50	4.00	2	100.00	626.72	-1.10	-6,112
3g (PQM-212)	>80	314.32	3.50	4.00	2	100.00	627.07	-1.10	-6,115
3h (PQM-213)	>80	314.32	3.51	4.00	2	96.98	581.29	-1.17	-6,265
3i (PQM-214)	4.94	330.77	3.76	4.00	2	100.00	626.88	-1.05	-6,147
3j (PQM-215)	48.43	330.77	3.76	4.00	2	100.00	626.71	-1.06	-6,155
3k (PQM-216)	35.29	330.77	3.76	4.00	2	100.00	579.69	-1.14	-6,318
3l (PQM-217)	4.46	375.22	3.83	4.00	2	100.00	627.03	-1.05	-6,183
3m (PQM-218)	28.95	352.43	4.54	4.00	2	100.00	606.96	-1.36	-6,222
3n (PQM-219)	>80	339.39	3.80	5.00	2	100.00	588.73	-1.41	-6,476
3o (PQM-220)	>80	367.45	4.39	5.00	2	100.00	592.84	-1.56	-6,512
3p (PQM-221)	30.59	386.40	3.66	6.25	2	100.00	717.41	-1.37	-5,88
3q (PQM-222)	>80	356.38	3.59	5.50	2	100.00	721.74	-1.30	-6,056
3r (PQM-223)	>80	379.46	4.58	5.00	2	100.00	623.78	-1.36	-6,653
3s (PQM-224)	16.75	365.43	4.16	5.00	2	100.00	586.96	-1.34	-6,383
3t (PQM-225)	>80	381.43	3.61	6.70	2	100.00	604.41	-1.34	-6,469
3u (PQM-226)	>80	362.39	3.62	5.50	2	92.66	307.91	-1.65	-6,972
3v (PQM-227)	>80	374.40	2.95	7.00	2	84.63	181.36	-2.05	-7,194
3w (PQM-228)	33.9	340.34	2.85	5.50	2	93.67	626.57	-1.16	-5,699
4a (PQM-196)	17.78	296.33	3.16	4.00	2	96.13	680.46	-1.17	-6,234
4b (PQM-197)	>80	312.32	2.39	4.75	3	82.43	208.13	-1.80	-6,099
4c (PQM-198)	>80	310.35	4.00	4.00	1	100.00	2224.37	-0.62	-6,16
4d (PQM-199)	24.6	340.38	4.00	4.75	1	100.00	2364.62	-0.65	-5,908
4e (PQM-200)	>80	326.35	3.25	4.75	2	100.00	769.67	-1.17	-5,985

[a]Concentration resulting in 50% inhibition of neuronal viability in SH-SY5Y cells. [b]ADME parameters: QPlogP - o/w-Predicted octanol/water partition coefficient (-2.0 to 6.5); HBA - Hydrogen bonding acceptors (2 to 20); HBD - Hydrogen bonding donor (0 to 6); % HOA-Percentage of human absorption by oral route (<25%-low; >80%-high); QPPCaco - Permeability in Caco cell assay, a model for intestinal absorption (<25–low; >500–high); QPlogBB - Permeability in the blood-brain barrier (-3.0 to 1.2).

2.3.Antioxidant and Metal Chelating Activity

ROS overload is a pathogenetic event that triggers OS and neuronal death during the neurodegenerative processes of PD. Therefore, we evaluated the direct and indirect antioxidant activity

of the *N*-aryl-cinnamoyl-hydrazone derivatives, in terms of their ability to scavenge the radical species and increase the intracellular antioxidant defense, respectively, in SH-SY5Y cells.

Initially, the direct antioxidant activities of the target compounds were determined against the DPPH radical in the absence of neuronal cells in different concentrations (200-1.56 mg/L) to calculate the EC_{50} (concentration required to obtain a 50% antioxidant effect). All compounds synthesized from ferulic acid (**3a–h**, **3n–o**, **3q–r,** and **3t-v**) showed the ability to scavenge the DPPH radicals. Among these, compounds **3e** (PQM-164), **3h** (PQM-213), and **3t** (PQM-225) recorded the highest antioxidant activities with EC_{50} values of 0.9, 7.7, and 8.9 μM, respectively (Table 2). Conversely, the series of compounds obtained from 4-methoxy cinnamic acid, **4b-c** and **4e**, did not exert any antioxidant activity against the DPPH radicals. As expected, the significant increase in free radical scavenging capacity exhibited for the 4-hydroxy-substituted derivatives (series 3) in comparison to the 4-methoxy-substituted analogues (series 4) is attributed to the highest ability 4-hydroxy group in the formation of a resonant stabilized phenoxy radical. Thus, we concluded that the 4-hydroxy-3-methoxy substitution pattern on the aromatic ring of ferulic acid is indispensable for antioxidant activity. This becomes even clearer when verifying that compound **3e**, which exhibits this same substitution pattern in the two aromatic subunits, exhibited the highest direct antioxidant activity, being 7.7 and 9.8-fold more potent than compounds **3h** and **3t**, respectively, the second and third best antioxidants in the series. Similarly to these results, Dias et.al. have previously reported a comparative study of the antioxidant activity between two series of ferulic and iso-ferulic acid derivatives, highlighting the central pharmacophoric role of the ferulic acid substitution pattern for good antioxidant activity [36].

Subsequently, we determined the direct antioxidant activity of the *N*-aryl-cinnamoyl-hydrazone derivatives against the ROS formation induced by pro-oxidant *t*-BOOH in neuronal cells. The SH-SY5Y cells were treated with 100 μM *t*-BOOH in the presence of 10 μM of the tested compounds for 30 min, and then the ROS formation was evaluated by fluorescent probe DCF-DA. Compounds **3a**–**h**, **3o**, **3t-v**, **4b** and **4e**, but not **3n**, **3q-r**,**4c** reduced the ROS formation elicited by *t*-BOOH in SH-SY5Y cells. Particularly, compounds **3b** (PQM-161), **3d** (PQM-163), **3e** (PQM-164), and **3t** (PQM-225) recorded a higher antioxidant activity than 75% (expressed as % inhibition of ROS formation). Remarkably, these compounds also showed the best submicromolar cellular antioxidant potencies (**3b**, EC_{50} = 0.71 μM; **3d**, EC_{50} = 0.20 μM; **3e**, EC_{50} = 0.51 μM; **3t**, EC_{50} = 0.81 μM).

In parallel, we also treated the SH-SY5Y cells with the tested compounds 24 hours before the treatment with *t*-BOOH to evaluate their indirect antioxidant activity. Among the evaluated compounds, only **3b** (PQM-161) and **3e** (PQM-164) were able to inhibit the ROS formation induced by *t*-BOOH in 24.8%, and 27.1%, respectively, suggesting their ability to activate endogenous antioxidant mechanisms.

Iron (Fe^{2+}) and copper (Cu^{2+}) metabolism are closely associated with OS in PD. Particularly, Fe^{2+} can act as a catalyst in the Fenton reaction and potentiates H_2O_2 neurotoxicity by generating a wide range of free radical species, including hydroxyl radicals (·OH) [37]. In this context, due to their direct antioxidant activity against t-BOOH in SH-SY5Y cells greater than 60%, we selected compounds **3b**, **3d-e**, **3g**, **3t**, **3u,** and **3v** to evaluate their additional ability to counteract the ROS formation evoked by Fenton reaction in SH-SY5Y cells using H_2O_2 and $FeSO_4$. At a concentration of 10 μM, all compounds showed the ability to decrease the ROS formation elicited by the Fenton reaction with a maximum inhibition of 80, 88, and 82%, for compounds **3d**, **3e,** and **3t**, respectively (Table 2).

Considering that curcumin, a structurally related ferulic acid dimmer, is widely reported for its significant metal-chelating ability [38], we decided to investigate such similar activity in our hybrid derivatives. Thus, an *in vitro* assay was carried out in which a solution with the three most antioxidant derivatives **3d**, **3e,** and **3t** at 20 μM was placed in contact with different Fe^{2+}, Fe^{3+}, Zn^{2+}, and Cu^{2+} solutions and the absorption spectrum was obtained in the UV-vis. The shift of the spectrum absorption curve of the pure compounds (Figure 3) relative to the curves obtained from the solutions of the compounds with the different metals is indicative of chelating activity [39]. Considering the literature data on chelating activity for curcumin [38], we could assume that compounds **3d**, **3e,** and **3t** were able to chelate all evaluated metals. Based on these results, it is plausible to suggest that both antioxidant activity and the inhibition of the Fenton reaction of the target compounds are due to a synergy of free radical stabilizing and metal chelating activities.

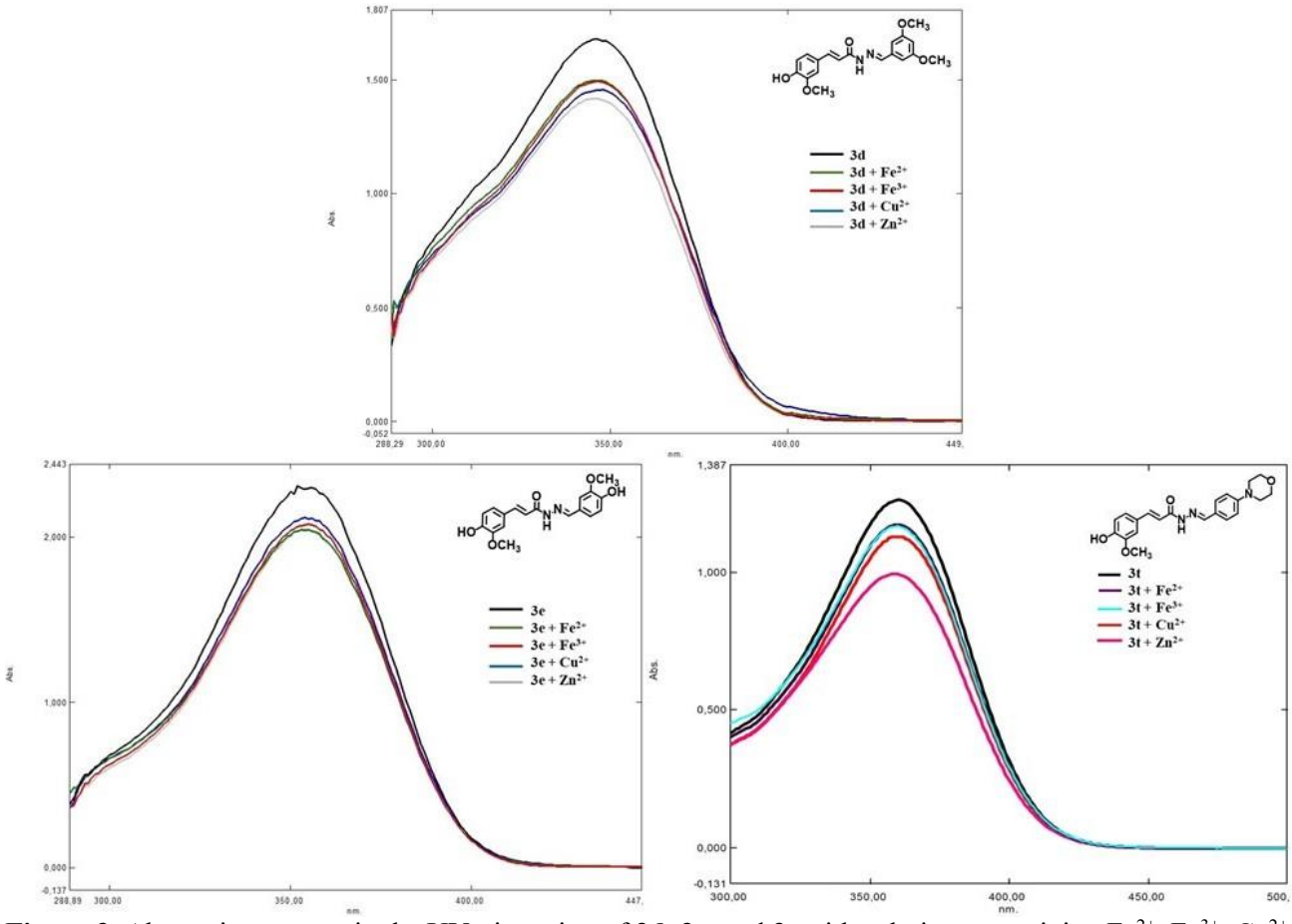

Figure 3. Absorption spectra in the UV-vis region of **3d**, **3e,** and **3t** with solutions containing Fe^{2+}, Fe^{3+}, Cu^{2+} e Zn^{2+}.

2.4. Monoamine oxidase (MAO) inhibition

Monoamine oxidase B (MAO-B) inhibition has been considered an effective treatment for PD, both as monotherapy or adjunct to levodopa. Whereas MAO-B is the main MAO isoform involved in dopamine metabolism in the human brain, MAO-A plays a role in that process, suggesting that it might alleviate some of the motor features of PD [7]. Thus, compounds **3b**, **3d-e**, **3t,** and **4b** were evaluated as inhibitors of the human MAO-A and MAO-B isoforms at 10 µM concentration. All feruloyl-based derivatives showed selective MAO-A inhibition higher than 30%, with compound **3d** exhibiting a maximum inhibition of 64%, in comparison to safinamide ($IC_{50\ MAO\text{-}B}$= 0.03 µM) and clorgyline ($IC_{50\ MAO\text{-}A}$= 0.02 µM) as positive controls. Compounds **3b** and **3d** showed 1.45- and 1.36-fold higher MAO-A/MAO-B selectivity, respectively. By contrast, the 4-methoxy cinnamic acid derivative **4b** exhibited a 1.76-fold higher selectivity for MAO-B, with an inhibition of 53% at 10 µM concentration (Table 2).

Table 2. Antioxidant activity on neuronal SH-SY5Y cells and Inhibitory activity on human MAO enzymes of selected *N*-aryl-cinnamoyl-hydrazone derivatives **3a-h**, **3n-o**, **3q-r**, **3t-v**, **4b-c,** and **4e**

Compound	DPPH EC_{50} (μM)[a]	Direct antioxidant activity *vs* t-BOOH in SH-SY5Y cells (%)[b]	Indirect antioxidant activity *vs* t-BOOH in SH-SY5Y cells (%)[c]	Direct antioxidant activity *vs* H_2O_2 + $FeSO_4$ in SH-SY5Y cells (%)[d]	*h*MAO-A inhibition (%)[e]	*h*MAO-B inhibition (%)[e]
3a	35	50	In	-	-	-
3b	20	76	25	53	55	38
3c	25	56	In	-	-	-
3d	30	75	In	80	64	47
3e	0.9	77	27	88	49	43
3f	43	38	In	-	-	-
3g	28	61	In	53	-	-
3h	7.7	57	In	-	-	-
3n	24	In	In	-	-	-
3o	22	41	In	-	-	-
3q	66	In	In	-	-	-
3r	38	In	In	-	-	-
3t	8.9	77	In	82	39	39
3u	25	63	In	66	-	-
3v	22	68	In	54	-	-
4b	In	46	In	-	30	53
4c	In	In	In	-	-	-
4e	In	24	In	-	-	-
Safinamide					18	(0.03 μM)
Clorgyline					(0.002 μM)	2

[a] The antioxidant activity is expressed as 50% inhibition of the DPPH radical; [b] % inhibition of ROS formation induced by t-BOOH in SH-SY5Y cells after simultaneous treatment with the compound (10 μM) and t-BOOH (100 μM); [c] % inhibition of ROS formation induced by t-BOOH in SH-SY5Y cells after a long treatment (24 h) with the compound (10 μM) and subsequent treatment with t-BOOH (100 μM); [d] % inhibition of ROS formation induced by $FeSO_4/H_2O_2$ in SH-SY5Y cells after a simultaneously treatment with the compound (10 μM) and $FeSO_4/H_2O_2$ (25 μM/100 μM); [e] % inhibition at 10 μM concentration. Safinamide and clorgyline were used as positive control (IC50 values in round brackets) [40]; In= inactive.

2.5. Neuroprotective activity in an in vitro model of PD

Neuroprotective effects of compounds **3b-e** were evaluated in SH-SY5Y cells treated with 6-hydroxydopamine (6-OHDA), a neurotoxin used to induce an *in vitro* PD model [41]. It is well known that 6-OHDA can trigger large OS and consequently impair dopaminergic neurons, as well as neuroinflammation both in *in vitro* and *in vivo* models, mimicking PD in humans [41]. Thus, we applied the same treatment approach used to assess the direct antioxidant activity of compounds **3b-e** in SH-SY5Y cells. Therefore, SH-SY5Y cells were treated with 6-OHDA (100 μM) and compounds (2.5 μM) for 2 hours and starved in a complete medium for 22 hours. The neurotoxicity was then evaluated by MTT assay. As shown in Figure 4, compounds **3b**, **3d,** and **3e**, but not **3c**, showed the ability to counteract the neurotoxicity induced by 6-OHDA. The SH-SY5Y cells were also submitted

to a pre-treatment with the compounds (2.5 μM) for 24 hours before the treatment with 6-OHDA. As a result, this treatment approach evidenced that **3b** and **3e**, but not **3c** and **3d**, reduced the neurotoxicity elicited by 6-OHDA. Overall, the neuroprotective effects of the compounds **3b** and **3e** show to resemble the antioxidant effects recorded in SH-SY5Y cells. These results confirm the highest direct antioxidant activity of **3b**, **3d,** and **3e** recorded in SH-SY5Y cells.

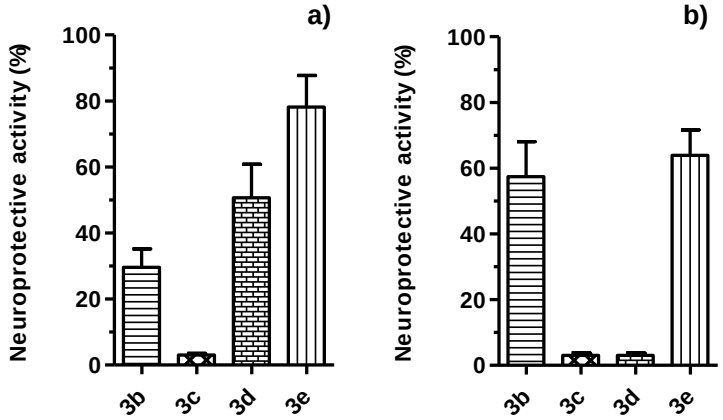

Figure 4. Effects of compounds **3b**, **3d**, **3c,** and **3e** on 6-OHDA induced neurotoxicity in SH-SY5Y cells. a) Cells were treated with compounds (2.5 μM) and 6-OHDA (100 μM) for 2 h and starved in complete medium for 22 h; b) Cells were treated with compounds (2.5 μM) for 24 h before the treatment with 6-OHDA (100 μM) for 2 h and starved in complete medium for 22 h. At the end of the treatments, the neurotoxicity was measured by MTT assay, as described in the experimental section. Data are expressed as neuroprotective activity (percentages of inhibition of neurotoxicity induced by 6-OHDA) and reported as mean ± SEM of at least three independent experiments.

Sporadic PD is associated with the formation and deposition of structures known as Lewy bodies that contain pathological (oligomeric, filamentous, or phosphorylated) forms of α-synuclein, α-synuclein–interacting protein, synphilin-1, and Pael-R (G protein–coupled receptor 37) [24,28,31,32]. To study the effects of compounds **3b** and **3e**, on α-synuclein aggregation, we used SH-SY5Y cells engineered to overexpress a green fluorescent protein (GFP)–tagged α-synuclein protein (designated TagGTP2-α-synuclein SH-SY5Y). TagGFP2-α-syn SH-SY5Y cells were treated with compounds (2.5 μM) and 6-OHDA (100 μM) for 2 h. After the treatment, the presence of α-syn aggregates was visualized by fluorescence microscopy analysis and quantified (Figure 5). Compound **3e**, but not **3b**, showed the ability to significantly decrease the levels of neurotoxic α-syn aggregates elicited by 6-OHDA.

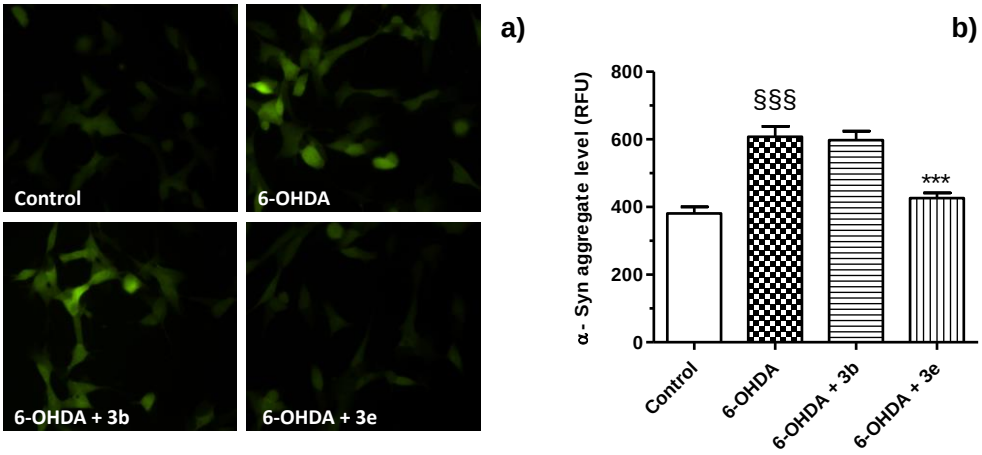

Figure 5. Effects of compounds **3b** and **3e** on α-syn aggregates induced by 6-OHDA in TagGFP2-α-syn SH-SY5Y cells. Cells were treated with compounds (2.5 μM) and 6-OHDA (100 μM) for 2 h. At the end of incubation, the α-syn aggregates level was detected by fluorescence microscope. (A) Representative images of α-syn aggregates. Scale bars: 50 μm. (B) Quantification of the α-syn aggregates level. Data are expressed as mean relative fluorescence units (RFU) ± SEM of at least three independent experiments (§§§$p < 0.001$ vs untreated cells, ***$p < 0.001$ vs cells treated with 6-OHDA a one-way ANOVA with the Bonferroni post hoc test).

Among several putative factors that may contribute to PD pathogenesis, inflammatory mechanisms may play a pivotal role. The involvement of microglial activation as well as of brain and peripheral immune mediators in PD pathophysiology has been reported by clinical and experimental studies [42,43]. The gene expression of iNOS and pro-inflammatory cytokines, including Interleukin 1β (IL-1β) and tumor necrosis factor α (TNF-α), was evaluated in microglial THP-1 cells after 24 h of treatment with LPS (1 μg/mL) in the presence of **3b** and **3e** (10 μM) by RT-PCR. As reported in Figure 6, compound **3e** significantly decreased iNOS, IL-1β, and TNF-α levels, whereas **3b** did not show effects on COX-2 expression.

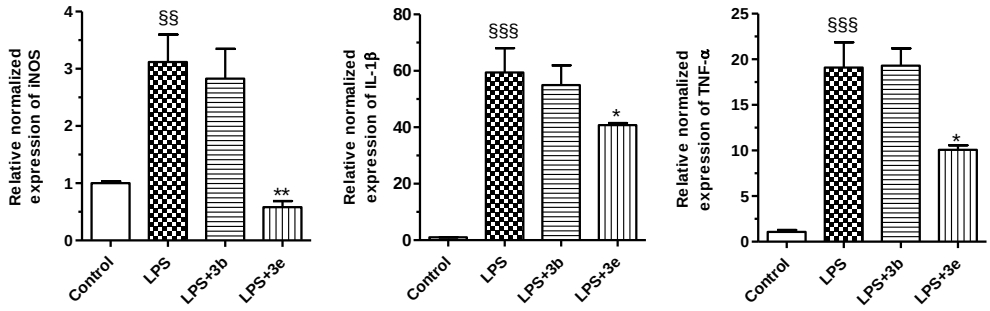

Figure 6. Effects of compounds **3b** and **3e** against LPS-induced inflammation in microglial THP-1 cells. Cells were incubated with compounds (10 μM) and LPS (1 μg/mL) for 24 h. At the end of incubation, iNOS, IL-1β, and COX-2 expression was measured by quantitative RT-PCR. Data are reported as mean ± SEM of three

independent experiments (§§§p<0.001 and §§p<0.01 vs untreated cells; **p<0.01 and *p<0.05 vs cells treated with LPS at one-way ANOVA with Bonferroni post hoc test).

2.6.Activation of the Nrf2/ARE Pathway and upregulation of GSH

Emerging evidence has suggested that the Nrf2/ARE pathway plays a crucial role in cellular adaption by controlling orchestrated cytoprotective proteins, including GSH, which is one of the main endogenous antioxidants, playing a critical role in protecting cells against OS damage [12,44,45] [13,49,50]. By observing the reduction of ROS levels and neurotoxicity following long-term treatment with compounds **3b** and **3e** before the treatment with t-BuOOH and 6-OHDA, respectively, we hypothesized that the antioxidant effect might likely result from an increase in GSH levels through the activation of the Nrf2/ARE Pathway. First, the Nrf2/ARE binding activity was studied in SH-SY5Y cells after increasing treatment times with **3b** and **3e** (2.5 μM) by a Nrf2 DNA-binding ELISA for activated Nrf2 transcription factor. It was evidenced that compound **3b**, as well as **3e** significantly increased the Nrf2 binding to the ARE sequence at the nuclear level after both short-term (3 h) and long-term treatments (12 h), with the highest activity after short-term treatment (Figure 7A). To confirm the increase in Nrf2 transcriptional activity upon treatment with **3b** and **3e**, the mRNA levels of NAD(P)H quinone dehydrogenase 1 (NQO1, enzyme involved in protection against OS), and glutathione synthetase (GSS, enzyme involved in the GSH biosynthesis pathway), both target of Nrf2 gene, were evaluated in SH-SY5Y cells by RT-PCR. As reported in Figures 7B and 7C, the 24-hour long-term treatment resulted in a significant ability of the tested compounds (2.5 μM) to increase both NQO1 and GSS expression genes. The intracellular GSH levels were also analyzed by employing the same experimental conditions by fluorescent probe monochlorobimane (MCB). Remarkably, the long-term treatment with **3b** and **3e** determined a significant increase in intracellular GSH levels (Figure 7D), suggesting that the antioxidant effects of these compounds could likely be ascribed to their ability to activate the Nrf2 pathway and, in turn, the transcription of GSH.

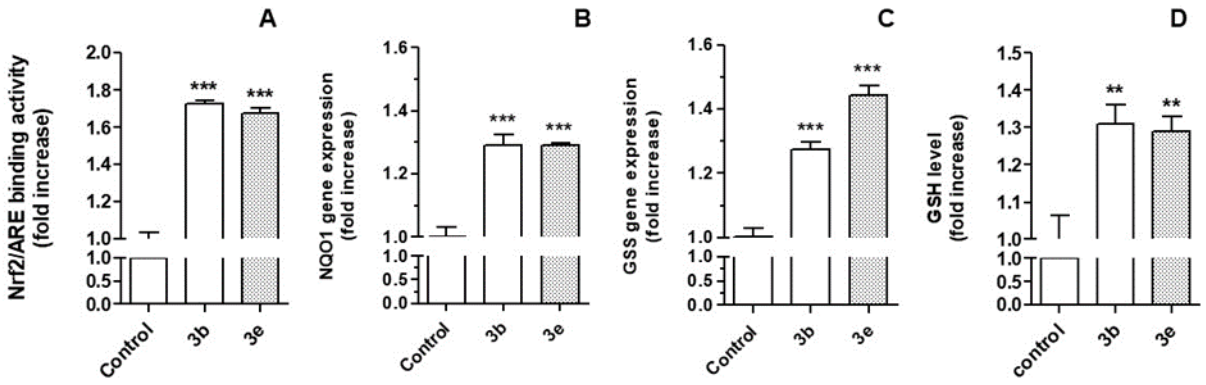

Figure 7. Effects of compounds **3b** and **3e** on the Nrf2/ARE binding activity, NQO1 and GSS gene expression, and GSH level in SH-SY5Y cells. (A) Cells were treated with compounds (2.5 μM) for 3h. The Nrf2/ARE binding activity was then determined by an ELISA assay; (B and C) cells were treated with compounds (2.5 μM) for 24 h. The NQO1 and GSS gene expression was then determined by RT-PCR; (D) cells were treated with compounds (2.5 μM) for 24 h. The GSH level was then determined by probe MCB. Results are expressed as mean ± SEM of at least three independent experiments (**$p < 0.01$ and ***$p < 0.001$ versus untreated cells at one-way ANOVA with the Dunnett post hoc test).

2.7. Docking Studies on Keap1

To evaluate the possible mode of action of the two lead compounds **3b** (PQM-161) and **3e** (PQM-164) and to rationalize their effect on the Keap1/Nrf2 system, in silico studies including docking and molecular dynamics (MD) simulations were performed. The Keap1 protein is known to be inactivated by small molecules with electrophilic character (e.g. Michael acceptors) like **3b** and **3e**, which would bind to the protein through the formation of covalent adducts at reactive cysteine residues [14]. In particular, the specific residue C151 of Keap1 BTB (Broad complex, Tramtrack, and Bric-a-Brac) domain was shown to be essential for the protein activity, since the C151W mutant Keap1 was found to be constitutively inactive [46]. Moreover, few Keap1 inhibitors and Nrf2 activators have been recently co-crystallized with Keap1 BTB domain covalently bound to C151 [46–48] or demonstrated to activate Nrf2/ARE pathway by uniquely binding C151 through the formation of a covalent adduct [49]. Based on these considerations, we hypothesized that **3b** and **3e** could reasonably interact with C151 of Keap1 BTB domain by acting as Michael acceptors similarly to the co-crystallized covalent inhibitors bearing α, β-unsaturated carbonyl moieties. For this reason, molecular docking studies were used to predict the formation of the covalent adducts produced by the Michael addition of the thiol group of C151 from the Keap1 BTB domain to the β unsaturated carbon of the ligands. Due to the high structural similarity of the two compounds, only **3b** was analyzed and the structure of the human BTB domain of Keap1 in complex with the covalent ligand CDDO (PDB code 4CXT) was used for this study [46]. The covalent docking protocol implemented in Gold software was applied to evaluate the binding orientations of the ligand after the formation of the covalent adduct with C151. The docking procedure generated 5 possible ligand binding dispositions, which were further studied by subjecting the 5 corresponding ligand-protein covalent complexes to 30 ns of MD simulations in an explicit water environment (see Materials and Methods for details). The results were then analyzed in terms of ligand-protein interaction energy, to evaluate the reliability of the predicted covalent adducts from an energetic point of view. For this purpose, the linear interaction energy (LIE) approach was employed.

LIE evaluations allow to calculate the non-bonded interactions between the ligand and the surrounding protein residues from the trajectories generated through MD simulations. Electrostatic and van der Waals energetic contributions are calculated for each MD snapshot and the obtained values are then used to derive the average total ligand-protein interaction energy. The MD trajectories extracted from the last 10 ns of MD simulation were used for the calculations, for a total of 100 snapshots (with a time interval of 100 ps). The average LIE values (aLIE) obtained for the different ligand-protein complexes formed by the covalent addition of **3b** to C151 of the Keap1 BTB domain are reported in Table 3 as the sum of the average electrostatic (EELE) and van der Waals (EVDW) energy contributions expressed as kcal/mol.

Table 3. Linear Interaction Energy (LIE) results for the ligand-protein complexes formed by covalent addiction of **3b** (PQM-161) to C151 of Keap1 BTB domain. Data are expressed as kcal/mol.

Binding pose	EELE	EVDW	aLIE
1	-7.1	-23.5	-30.6
2	-7.0	-24.5	-31.5
3	-13.5	-22.8	-36.4
4	3.2	-24.2	-21.0
5	-13.0	-18.3	-31.2

LIE calculations suggested binding pose 3 as the most energetically favored covalent adduct, showing an average value of total energy (-36.4 kcal/mol) exceeding about a minimum of 5 kcal/mol up to more than 15 kcal/mol those associated with the other covalent complexes predicted by docking procedure. In figure 8, it is depicted the average binding pose 3 of compound **3b** covalently bound to the C151 residue of Keap1 obtained from the last 10 ns of MD simulation.

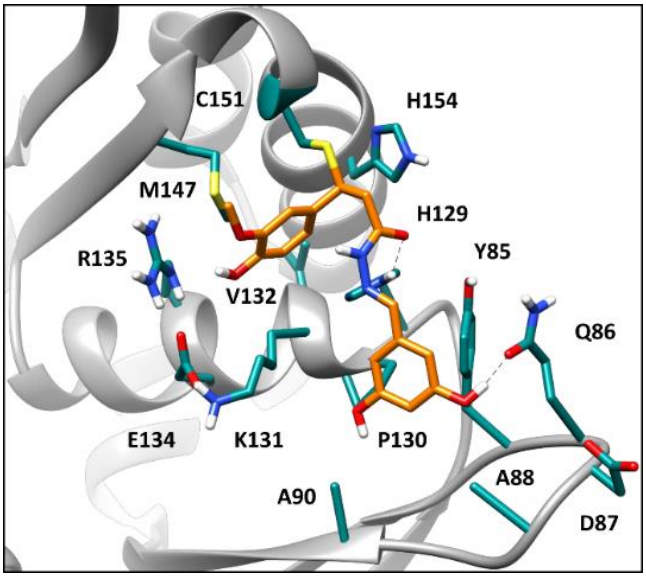

Figure 8: Minimized average structure of the Keap1 BTB domain with compound **3b** covalently bound to C151 residue. The covalent ligand is shown in orange, while the protein residues are colored dark cyan.

The methoxyphenol moiety of the ligand **3b** (PQM-161) directly linked to the alkylated carbon is placed in a quite big ellipsoidal-shaped pocket adjacent to C151, formed by H129, K131, V132, E134, R135, M147 and H154. In particular, the ligand forms stable hydrophobic interactions with H129 and the carbon chain of K131, as well as with M147, which are localized in the lower and upper side of the pocket, respectively. Conversely, the benzene-1,3-dihydroxilated subunit of the ligand **3b** lies on a more solvent-exposed pocket mainly delimited by Y85, Q86, D87, A88, A90, H129 and P130 and forms lipophilic interactions with these pocket residues. Moreover, a T-shaped stacking interaction with Y85 and an H-bond with the side chain of Q86 were observed. Finally, an additional H-bond is formed between the carbonyl oxygen of the ligand and H129.

3. Experimental section

3.1. Chemistry

The IR spectra have been generated in an infrared spectrometer Nicolet iSso (Thermo scientific USA) coupled to Pike Gladi ATR technologies in the Laboratory of Analysis and Characterization of Drugs (LACFar) at the Federal University of Alfenas (UNIFAL-MG). The ^{1}H and ^{13}C NMR spectra were obtained on a Bruker AC-300 spectrometer operating at 300 MHz for ^{1}H NMR and 75 MHz for ^{13}C NMR in the Laboratory of Nuclear Magnetic Resonance at the UNIFAL-MG. All reagents used in synthesis were purchased from Sigma-Aldrich without further purification. Thin layer chromatography experiments were performed on silica gel sheet 60 F254 (Merck), and purification by chromatography

column was performed on flash silica gel (220‑440 mesh, 0.035mm‑0.075 mm, Sigma-Aldrich). The visualization of the substances was performed in a UV chamber (λ=254 or 365 nm). The solvents dichloromethane, ethanol, and dimethylformamide were treated, distilled, and dried according to the literature [50]. Melting points were set on Mars equipment (PFM II) with crushed samples and packaged in capillary tubes without correction. All spectra, including those related to intermediate compounds, are available in the supplementary material. Purity of the final compounds was determined by HPLC in a Shimadzu equipment and *In silico* prediction of ADME parameters was obtained using QikProb 3.1 software developed by Schrodinger® (New York, USA).

3.1.1. General procedure for the preparation of hydrazides 6a and 6b.

To a solution of ferulic acid or 4-methoxy-cinnamic acid (1.68 mmol) in 10 mL of acetonitrile was added HOBT (2.02 mmol) and EDAC (2.02 mmol). The solution was stirred at approximately 25 °C for 1.5 hours. Then, a solution of hydrazine monohydrate (16.8 mmol) in 5 mL of acetonitrile was prepared and cooled in an ice bath to approximately 0 °C. The first solution was added drop-to-drop to the second, while the system was kept in an ice bath. When the reaction was completed (TLC), the solvent was evaporated, and the crude reaction mixture was resuspended in 4 mL of 5% saturated $NaHCO_3$ and the final solution was kept in a freezer for 6 h. The precipitate formed was filtrated and washed with cold water to furnish hydrazides **6a** or **6b** as white/pale solids.

3.1.2. General procedure for the coupling reaction of hydrazides 6a/6b with substituted aldehydes for the preparation of series 3 and 4.

To a solution of the corresponding hydrazide derivative (**6a**, 0.48 mmol or **6b**, 0.52 mmol) in dry ethanol (10 mL) containing a catalytic amount of 40% HCl aq. was added to 0.62 mmol of adequate benzaldehyde. The reaction mixture was stirred at 25 °C for 24 h. After confirmation of the completion of the reaction (TLC), the solvent was removed under reduced pressure, and cold ethanol was added. The solid formed was collected by filtration. When necessary, the product was purified by silica gel flash column chromatography.

3.1.3. (*E*)-3-(4-hydroxy-3-methoxyphenyl)-*N*'-(4-hydroxybenzylidene)acrylohydrazide (3a, PQM-160).

Yellow solid (yield 78%), m.p. 262 ºC, purity: 99.3 % (HPLC). IR (ATR): ν 3075.42, 3014.19, 2921.63, 2828.10, 1678.73, 1606.41, 1580.38, 1455.99, 1350.89 and 1102.60 cm^{-1}. ^1H NMR (300 MHz, DMSO-*d6*) δ 11.41 and 11.17 (*s*, 1H, N-N<u>H</u>), 9.53 (*s*, 1H, O<u>H</u>), 8.55 (*s*, 1H, O<u>H</u>), 8.12 and 7.95

(*s*, 1H, N=C<u>H</u>), 7.69 (*d*, *J*= 8.63 Hz, 2H, Ar-<u>H</u>), 7.63–7.54 (*m*, 2H, Ar-<u>H</u>), 7.51 and 7.37 (*d*, *J*=15.11 and 15.95 Hz, 1H, <u>H</u>C=CH), 7.26 and 7.18 (*s*, 1H, Ar-<u>H</u>), 7.06 (*d*, *J* = 7.11 Hz, 1H, Ar-<u>H</u>), 6.91–6.78 (*m*, 6H, Ar-<u>H</u>), 6.49 (*d*, *J* = 15.11 Hz, 1H, HC=C<u>H</u>) and 3.85 and 3.82 (*s*, 3H, C<u>H</u>$_3$). ^{13}C NMR (75 MHz, DMSO-*d6*) δ 166.3, 161.8, 160.4, 147.9, 146.5, 143.2, 130.2, 128.9, 128.7, 126.3, 125.2, 121.9, 115.8, 111.0, and 55.6. HRMS (ESI) *m/z*: Calcd for $C_{17}H_{17}N_2O_4$ $[M+H]^+$ 313.1188, found 313.1187. Calcd for $C_{17}H_{16}N_2NaO_4$ $[M+Na]^+$ 335.1008, found 335.1009.

3.1.4. (*E*)-*N*'-(3,5-dihydroxybenzylidene)-3-(4-hydroxy-3-methoxyphenyl)-acrylohydrazide (3b, PQM-161).

Brown solid (yield 27%), m.p. 232 ºC, purity: 99.3 % (HPLC). IR (ATR): ν 3374.39, 3230.23, 3047.03, 2962.17, 1622.83, 1585.23, 1467.11, 1343.68 and 1018.73 cm^{-1}. ^{1}H NMR (300 MHz, CD_3OD) δ 7.96 and 7.82 (s, 1H, N=C<u>H</u>), 7.66 and 7.43 (*d*, *J* = 15.41 e 15.64 Hz, 1H, <u>H</u>C=CH), 7.16 (*d*, *J* = 1.31 Hz, 1H, Ar-<u>H</u>), 7.09 (*dd*, *J* = 1.31, 8.07 Hz, 1H, Ar-<u>H</u>), 6.82 (*d*, *J* = 8.07 Hz, 1H, Ar-<u>H</u>), 6.72 (*d*, *J* = 2.17 Hz, 2H, Ar-<u>H</u>), 6.47 (*d*, *J* = 15.41 Hz, 1H, HC=C<u>H</u>), 6.32 (*s*, 1H, Ar-<u>H</u>), 3.90 (*s*, 3H, C<u>H</u>$_3$) and 3.35 (*s*, 2H, O<u>H</u>). ^{13}C NMR (75 MHz, CD_3OD) δ 165.8, 160.0, 149.6, 149.4, 146.0, 145.1, 144.3, 137.3, 128.3, 123.6, 123.4, 116.6, 111.8, 107.1, and 55.5. HRMS (ESI) *m/z*: Calcd for $C_{17}H_{17}N_2O_5$ $[M+H]^+$ 329.1137, found 329.1141. Calcd for $C_{17}H_{16}N_2NaO_5$ $[M+Na]^+$ 351.0957, found 351.0957.

3.1.5. (*E*)-3-(4-hydroxy-3-methoxyphenyl)-*N*'-(4-methoxybenzylidene)acrylohydrazide (3c, PQM-162)

Light yellow solid (Yield 53%), m.p. 226 ºC, purity: 99.9 % (HPLC). IR (ATR) ν 3116.40, 3046.50, 2928.86, 2833.40, 1651.25, 1605.63, 1507.58, 1420.80, 1398.14 and 1031.25 cm^{-1}. ^{1}H NMR (300 MHz, CD_3OD) δ 88.08 and 7.95 (*s*, 1H, N=C<u>H</u>), 7.75 (*d*, *J* = 8.83 Hz, 2H, Ar-<u>H</u>), 7.66 and 7.45 (*d*, *J* = 15.61 and 15.95 Hz, 1H, <u>H</u>C=CH), 7.17 (*d*, *J* = 1.81 Hz, 1H, Ar-<u>H</u>), 7.10 (*dd*, *J* = 1.81, 8.22 Hz, 1H, Ar-<u>H</u>), 6.97 (*d*, *J* = 8.86 Hz, 2H, Ar-<u>H</u>), 6.83 (*d*, *J* = 8.22 Hz, 1H, Ar-<u>H</u>), 6.48 (*d*, *J* = 15.61 Hz, 1H, HC=C<u>H</u>), 3.90 (*s*, 3H, C<u>H</u>$_3$) and 3.83 (*s*, 3H, C<u>H</u>$_3$). ^{13}C NMR (75 MHz, CD_3OD) δ 165.7, 163.2, 150.4, 149.3, 145.0, 144.0, 130.5, 129.8, 128.1, 123.5, 116.6, 116.4, 115.3, 111.8, 56.4 and 55.9. HRMS (ESI) m/z: Calcd for $C_{18}H_{19}N_2O_4$ $[M+H]^+$ 327.1345, found 327.1343. Calcd for $C_{18}H_{18}N_2NaO_4$ $[M+Na]^+$ 349.1164, found 349.1163.

3.1.6. (*E*)-*N*'-(3,5-dimethoxybenzylidene)-3-(4-hydroxy-3-methoxyphenyl)-acrylohydrazide (3d, PQM-163).

Beige solid (Yield 47%), m.p. 214 ºC, purity: 99.7 % (HPLC). IR (ATR) ν 3153.53, 3055.17, 2934.16, 2833.88, 1660.89, 1628.59, 1587.13, 1423.69, 1363.43, 1054.87 cm^{-1}. ^{1}H NMR (300 MHz, DMSO-*d6*) δ 11.43 and 11.21 (*s*, 1H, N-N<u>H</u>), 8.10 and 7.93 (*s*, 1H, N=C<u>H</u>), 7.50 (*d*, 1H, *J* = 15.67

MHz, HC=CH), 7.38 and 7.31 (*s*, 2H, Ar-H), 7.20–7.12 (*m*, 1H, Ar-H), 7.08 (*t*, 3H, Ar-H), 6.82 (*d*, *J* = 8.13 Hz, 3H, Ar-H), 6.51 (*d*, *J* = 15.67 MHz, HC=CH), 3.85 and 3.82 (*s*, 9H, CH_3). ^{13}C NMR (75 MHz, DMSO-*d6*) δ 162.0, 160.7, 149.0, 148.8, 146.1, 142.4, 141.2, 136.5, 126.2, 122.8, 122.0, 116.7, 115.7, 111.0, 104.8, 102.3, 55.5, 55.4, 55.2 and 55.0. HRMS (ESI) *m/z*: Calcd for $C_{19}H_{21}N_2O_5$ $[M+H]^+$ 357.1450, found 357.1453.

3.1.7. (*E*)-*N*'-(4-hydroxy-3-methoxybenzylidene)-3-(4-hydroxy-3-methoxyphenyl)-acrylohydrazide (3e, PQM-164).

Yellow solid (yield 48%), m.p. 157 ºC, purity: 99.9 % (HPLC). IR (ATR) ν 3212.34, 3059.03, 2965.02, 2840.15, 1651.73, 1585.20, 1427.55, 1373.55 and 1025.46 cm^{-1}. ^1H NMR (300 MHz, DMSO-*d6*) δ 11.35 and 11.16 (*s*, 1H, N-NH), 9.45 (*s*, 2H, OH), 8.04 and 7.87 (*s*, 1H, N=CH), 7.45 and 7.38 (*d*, *J* = 15.65 and 15.99 Hz, 1H, HC=CH), 7.32 and 7.24 (*s*, 1H, Ar-H), 7.01 (*t*, *J* = 6.77 Hz, 4H, Ar-H), 6.76 (*d*, *J* = 8.11 Hz, 4H, Ar-H), 6.44 (*d*, *J* = 15.65 Hz, 1H, HC=CH) and 3.76 (s, 12H, CH_3).^{13}C NMR (75 MHz, DMSO-*d6*) δ 166.2 and 161.7, 148.9, 148.7, 148.0, 147.9, 146.7 and 143.0, 140.7 and 114.1, 126.3, 125.8, 122.0, 121.9, 117.0, 115.7, 115.5, 111.0, 109.1 and 55.56. HRMS (ESI) *m/z*: Calcd for $C_{18}H_{19}N_2O_5$ $[M+H]^+$ 343.1288, found 343.1299.

3.1.8. (*E*)-*N*'-((*E*)-4-fluorobenzylidene)-3-(4-hydroxy-3-methoxyphenyl)-acrylohydrazide (3f, PQM-211).

Yellow solid (yield 67%), m.p. 138 ºC, purity: 99.9 % (HPLC). IR (ATR): ν 3310, 3170, 3007, 2897, 1655, 1621, 1589 and 1372 cm^{-1}. ^1H NMR (300 MHz, DMSO- *d6*) δ 11.77 and 11.41 (*s*, 1H, NH), 8.23 and 8.04 (*s*, 1H, N=CH), 7.85 – 7.72 (*m*, 4H, Ar-H), 7.58 and 7.51 (*d*, *J* = 15.8 and 15.7 Hz, 1H, HC=CH), 7.38 and 6.56 (d, *J* = 15.8 and 15.7 Hz, 1H, HC=CH), 7.26 (t, *J* = 8.8 Hz, 4H, Ar-H), 7.26 and 7.18 (*d*, *J* = 1.4 and 1.5 Hz, 1H, Ar-H), 7.18 and 7.06 (*dd*, *J* = 1.4; 8,1 and 1.5; 8.0 Hz, 1H, Ar-H), 6.84 and 6.82 (*d*, *J* = 8.0 and 8.1 Hz, 1H, Ar-H), 3.83 and 3.80 (*s*, 3H, OCH_3). ^{13}C NMR (75 MHz, DMSO- *d6*) δ 166.95, 163.46 (*d*, *J* = 247.5 Hz), 162.46, 149.40, 149.29, 148.30, 145.37, 143.32, 142.11, 141.54, 131.50, 131.37, 129.64 (*d*, *J* = 8.2 Hz), 126.60, 126.53, 122.53, 122.41, 117.21, 116.33 (*d*, *J* = 21.8 Hz), 116.18, 114.02, 112.69, 111.14, 56.24 and 56.00. HRMS (ESI) *m/z*: Calcd for $C_{17}H_{16}FN_2O_3$ $[M+H]^+$ 315.1145, found 315.1141. Calcd for $C_{17}H_{15}FN_2NaO_3$ $[M+Na]^+$ 337.0964, found 337.0959.

3.1.9. (*E*)-*N*'-((*E*)-3-fluorobenzylidene)-3-(4-hydroxy-3-methoxyphenyl)-acrylohydrazide (3g, PQM-212).

Beige solid (yield 37%), m.p. 212 ºC, purity: 99.7 % (HPLC). IR (ATR): ν 3247, 3044, 2938, 1654, 1620, 1584 and 1383 cm^{-1}. ^1H NMR (300 MHz, DMSO- *d6*) δ 11.74 and 11.45 (*s*, 1H, NH), 9.55 (*s*, 2H, OH), 8.23 and 8.04 (*s*, 1H, N=CH), 7.60 and 7.39 (*d*, *J* = 16.1 and 15.9 Hz, 1H, HC=CH), 7.57

– 7.42 (*m*, 8H, Ar-H), 7.29 and 7.18 (*s*, 1H, Ar-H), 7.24 and 7.07 (*d*, *J* = 8.8 and 8.0 Hz, 1H, Ar-H), 7.23 and 6.53 (*d*, *J* = 16.1 and 15.9 Hz, 1H, HC=CH), 6.82 (*d*, *J* = 8.0 Hz, 2H, H-1), 3.83 and 3.81 (*s*, 3H, OCH_3). ^{13}C NMR (75 MHz, DMSO- *d*$_6$) δ 167.07, 162,89 (*d*, *J* = 243.8 Hz), 162.56, 149.43, 149.31, 148.31, 145.16, 143.51, 141.83, 137.54, 137.44, 131.30 (*d*, *J* = 8.2 Hz), 126.82, 126.58, 123.83, 122.65, 122.48, 117.06, 116.21, 113.95, 113.44 (*d*, *J* = 22.5 Hz), 113.27 (*d*, *J* = 22.4 Hz), 112.78, 111.51, 56.20 and 56.00. HRMS (ESI) *m/z*: Calcd for $C_{17}H_{16}FN_2O_3$ $[M+H]^+$ 315.1145, found 315.1145. Calcd for $C_{17}H_{15}FN_2NaO_3$ $[M+Na]^+$ 337.0964, found 337.0962.

3.1.10. (*E*)-*N*'-((*E*)-2-fluorobenzylidene)-3-(4-hydroxy-3-methoxyphenyl)-acrylohydrazide (3h, PQM-213).

Beige solid (yield 42%), m.p. 215 ºC, purity: 99.9 % (HPLC). IR (ATR): ν 3454, 3305, 3010, 2965, 1662, 1617, 1585 and 1370 cm^{-1}. ^1H NMR (300 MHz, DMSO- *d*$_6$) δ 11.98 and 11.52 (*s*, 1H, NH), 9.63 (*s*, 2H, OH), 8.46 and 8.24 (*s*, 1H, N=CH), 7.59 and 7.53 (*d*, *J* = 16.4 and 16.1 Hz, 1H, HC=CH), 7.37 and 6.54 (*d*, *J* = 16.4 and 16.1 Hz, 1H, HC=CH), 7.47 – 7.42 (*m*, 2H, Ar-H), 7.31 – 7,25 (*m*, 4H, Ar-H), 7,27 and 7.18 (*s*, 1H, Ar-H), 7.23 and 7.06 (*d*, *J* = 8.0 and 7.6 Hz, 1H, Ar-H), 6.84 and 6.82 (*d*, *J* = 8.0 and 7.6 Hz, 1H, Ar-H), 3.82 and 3.80 (*s*, 3H, OCH_3). ^{13}C NMR (75 MHz, DMSO- *d*$_6$) δ 166.99, 162,74, 160,97 (*d*, *J* = 230.67 Hz), 149.45, 149.29, 148.29, 143.55, 141.81, 139.13, 136.01, 132.29 (*d*, *J* = 8.1 Hz), 132.08, 131.97, 126.82 (*d*, *J* = 14.03 Hz), 125.41, 122.56, 122.45, 117.04, 116.23 (*d*, *J* = 21.45 Hz), 113.80, 113.29 (*d*, *J* = 8.1 Hz), 112.69, 111.51, 56.20 and 56.00. HRMS (ESI) *m/z* Calcd for $C_{17}H_{15}FN_2NaO_{34}$ $[M+Na]^+$ 337.0964, found 337.0972.

3.1.11. (*E*)-*N*'-((*E*)-4-chlorobenzylidene)-3-(4-hydroxy-3-methoxyphenyl)-acrylohydrazide (3i, PQM-214).

Yellow solid (yield 63%), m.p. 225 ºC, purity: 99.9 % (HPLC). IR (ATR): ν 3249, 3084, 2985, 1652, 1627, 1586 and 1351 cm^{-1}. ^1H NMR (300 MHz, DMSO- *d*$_6$) δ 11.64 and 11.43 (*s*, 1H, NH), 9.56 (*s*, 2H, OH), 8.18 and 8.02 (*s*, 1H, N=CH), 7.77 (*d*, *J* = 8.4 Hz, 2H, Ar-H), 7.72 (*d*, *J* = 8.5 Hz, 2H, Ar-H), 7.58 and 7.52 (*d*, *J* = 16.1 and 15.7 Hz, 1H, HC=CH), 7.36 and 6.50 (*d*, *J* = 16.1 and 15.7 Hz, 1H, HC=CH), 7.49 (*d*, *J* = 8.4 Hz, 4H, Ar-H), 7.27 and 7.18 (*s*, 1H, Ar-H), 7.21 and 7.06 (*d*, *J* = 8.1 Hz, 1H, Ar-H), 6.82 and 6.80 (*d*, *J* = 8.1 Hz, 1H, Ar-H), 3.83 and 3.80 (*s*, 3H, OCH_3). ^{13}C NMR (75 MHz, DMSO- *d*$_6$) δ 166.98, 162.44, 149.39, 149.25, 148.29, 145.18, 143.44, 141.93, 141.78, 134.78, 134.54, 133.83, 133.68, 129.35, 129.12, 126.79, 126.55, 122.51, 117.01, 116.17, 113.93, 112.70, 111.38, 56.21 and 55.95. HRMS (ESI) *m/z*: Calcd for $C_{17}H_{15}ClN_2NaO_3$ $[M+Na]^+$ 353.0669 found 353.0647.

3.1.12. (*E*)-*N*'-((*E*)-3-chlorobenzylidene)-3-(4-hydroxy-3-methoxyphenyl)-acrylohydrazide (3j, PQM-215).

White solid (yield 45%), m.p. 215 ºC, purity: 99.9 % (HPLC). IR (ATR): ν 3150, 3043, 2940, 1651, 1616, 1582 and 1381 cm^{-1}. NMR (300 MHz, DMSO- *d*$_6$) δ 11.68 and 11.46 (*s*, 1H, NH), 9.55

(*s*, 2H, OH), 8.18 and 8.01 (*s*, 1H, N=CH), 7.78 (*d*, *J* = 12.4 Hz, 2H, Ar-H), 7.72 – 7.63 (m, 2H, Ar-H), 7.58 and 7.53 (*d*, *J* = 15.9 and 16.0 Hz, 1H, HC=CH), 7.38 and 6.52 (*d*, *J* = 15.9 and 16.0 Hz, 1H, HC=CH), 7.45 (*d*, *J* = 8.1 Hz, 2H, Ar-H), 7.45 and 7.44 (*s*, 1H, Ar-H), 7.30 and 7.18 (*s*, 1H, Ar-H), 7.20 and 7.06 (*d*, *J* = 8.1 Hz, 1H, Ar-H), 6.81 (*d*, *J* = 8.1 Hz, 2H, Ar-H), 3.84 and 3.81 (*s*, 3H, OCH_3). ^{13}C NMR (75 MHz, DMSO- *d*$_6$) δ 167.08, 162.54, 149.42, 149.31, 148.32, 144.84, 143.46, 141.89, 141.60, 137.16, 137.01, 134.09, 131.15, 129.97, 129.80, 126.75, 126.57, 126.11, 122.75, 122.51, 116.99, 116.19, 113.99, 112.53, 111.49, 56.15 and 56.00. HRMS (ESI) *m/z*: Calcd for $C_{17}H_{16}ClN_2O_3$ $[M+H]^+$ 331.0849, found 331.0848. Calcd for $C_{17}H_{15}ClN_2NaO_3$ $[M+Na]^+$ 353.0669, found 353.0677.

3.1.13. (*E*)-*N*'-((*E*)-2-chlorobenzylidene)-3-(4-hydroxy-3-methoxyphenyl)-acrylohydrazide (3k, PQM-216).

Yellow solid (yield 46%), m.p. 230 ºC, purity: 99.9 % (HPLC). IR (ATR): ν 3478, 3278, 3011, 1666, 1621, 1599 and 1431 cm^{-1}. ^1H NMR (300 MHz, DMSO- *d*$_6$) δ 11.85 and 11.59 (*s*, 1H, NH), 9.60 (*s*, 2H, OH), 8.59 and 8.43 (*s*, 1H, N=CH), 8.18 – 8.09 and 8.08 – 7.93 (*m*, 2H, Ar-H), 7.61 and 7.56 (*d*, *J* = 16.0 and 15.7 Hz, 1H, HC=CH), 7.39 and 6.49 (*d*, *J* = 16.0 and 15.7 Hz, 1H, HC=CH), 7.52 – 7.49 (*m*, 2H, Ar-H), 7.42 (*d*, *J*= 5.6 Hz, 2H, Ar-H), 7.41 (*d*, *J*= 5.6 Hz, 2H, Ar-H), 7,29 and 7.20 (*s*, 1H, Ar-H), 7.22 and 7.08 (*d*, *J* = 8.1 and 7.9 Hz, 1H, Ar-H), 6.82 (*d*, *J* = 8.1 Hz, 2H, Ar-H), 3.82 and 3.81 (*s*, 3H, OCH_3). ^{13}C NMR (75 MHz, DMSO- *d*$_6$) δ 167.07, 162.59, 149.70, 149.36, 148.32, 143.61, 142.43, 141.95, 139.29, 134.46, 133.30, 132.05, 131.77, 131.52, 130.34, 128.05, 127.47, 127.33, 126.77, 126.54, 122.57, 122.49, 117.00, 113.86, 112.75, 111.58, 56.21 and 55.00. HRMS (ESI) *m/z*: Calcd for $C_{17}H_{15}ClN_2NaO_3$ $[M+Na]^+$ 353.0669, found 353.0663.

3.1.14. (*E*)-*N*'-((*E*)-4-bromobenzylidene)-3-(4-hydroxy-3-methoxyphenyl)-acrylohydrazide (3l, PQM-217).

Yellow solid (yield 67%), m.p. 224 ºC, purity: 98.1 % (HPLC). IR (ATR): ν 3403, 3263, 3009, 2903, 1651, 1620, 1587 and 1361 cm^{-1}. ^1H NMR (300 MHz, DMSO- *d*$_6$) δ 11.62 and 11.42 (*s*, 1H, NH), 9.53 (*s*, 2H, OH), 8.18 and 8.00 (*s*, 1H, N=CH), 7.74 – 7.61 (m, 8H, Ar-H), 7.62 and 7.53 (*d*, *J* = 15.9 and 15.6 Hz, 1H, HC=CH), 7.36 and 6.50 (*d*, *J* = 15.9 and 15.6 Hz, 1H, HC=CH), 7.27 and 7.18 (*s*, 1H, Ar-H), 7.21 and 7.06 (*d*, *J* = 8.0 and 7.9 Hz, 1H, Ar-H), 6.82 and 6.81 (*d*, *J* = 8.0 and 7.9 Hz, 1H, Ar-H), 3.83 and 3.81 (*s*, 3H, OCH_3). ^{13}C NMR (75 MHz, DMSO- *d*$_6$) δ 166.57, 162.18, 149.45, 149.29, 148.31, 145.24, 143.41, 142.01, 141.68, 134.21, 134.05, 132.25, 129.33, 126.80, 126.59, 123.53, 123.29, 122.55, 122.44, 117.16, 116.21, 113.96, 112.74, 111.51, 56.25, and 56.00. HRMS (ESI) *m/z*: Calcd for $C_{17}H_{16}BrN_2O_3$ $[M + H]^+$ 375.0344, found 375.0346. Calcd for $C_{17}H_{15}BrN_2NaO_3$ $[M+Na]^+$ 397.0164, found 397.0155.

3.1.15. (*E*)-*N*'-((*E*)-4-(tert-butyl)benzylidene)-3-(4-hydroxy-3-methoxyphenyl)-acrylohydrazide (3m, PQM-218).

Light green solid (yield 31%), m.p. 235 ºC, purity: 99.9 % (HPLC). IR (ATR): ν 3447, 3196, 3006, 2959, 3663, 1640, 1575 and 1365 cm^{-1}. ^{1}H NMR (300 MHz, DMSO- *d*$_6$) δ 11.50 and 11.31 (*s*, 1H, NH), 9.52 (*s*, 2H, OH), 8.17 and 8.01 (*s*, 1H, N=CH), 7.65 and 7.62 (*d*, *J* = 8.4 Hz, 2H, Ar-H), 7.58 and 7.52 (*d*, *J* = 15.7 Hz, 1H, HC=CH), 7.37 and 6.50 (*d*, *J* = 15.7 Hz, 1H, HC=CH), 7.44 (*d*, *J* = 8.4 Hz, 4H, Ar-H), 7.26 and 7.17 (*s*, 1H, Ar-H), 7.19 and 7.06 (*d*, *J* = 7.7 and 8.0 Hz, 1H, Ar-H), 6.82 and 6.80 (*d*, *J* = 7.7 and 8.0 Hz, 1H, Ar-H), 3.84 and 3.81 (*s*, 3H, OCH_3), 1.27 (*s*, 18H, C-CH_3). ^{13}C NMR (75 MHz, DMSO- *d*$_6$) δ 166.85, 162.34, 153.22, 152.93, 149.38, 149.21, 148.33, 146.55, 143.15, 141.48, 132.08, 127.35, 126.88, 126.66, 126.07, 122.52, 122.40, 117.26, 116.21, 114.18, 112.55, 111.48, 56.24, 56.01, 35.04, and 31.44. HRMS (ESI) *m/z*: Calcd for $C_{21}H_{25}N_2O_3$ $[M + H]^+$ 353.1865, found 353.1873. Calcd for $C_{21}H_{24}N_2NaO_3$ $[M+Na]^+$ 375.1685, found 375.1691.

3.1.16. (*E*)-*N*'-((*E*)-4-(dimethylamino)benzylidene)-3-(4-hydroxy-3-methoxyphenyl)-acrylohydrazide (3n, PQM-219).

Yellow solid (yield 53%), m.p. 121ºC, purity: 98.2 % (HPLC). IR (ATR): ν 3364, 2994, 2913, 1648, 1591, 1575 and 1372 cm^{-1}. ^{1}H NMR (300 MHz, DMSO- *d*$_6$) δ 11.81 and 11.31 (*s*, 1H, NH), 9.67 (*s*, 2H, OH), 8.23 and 8.03 (*s*, 1H, N=CH), 7.76 – 7.64 (*m*, 4H, Ar-H), 7.56 and 7.51 (*d*, *J* = 15.3 and 15.6 Hz, 1H, HC=CH), 7.40 and 6.64 (*d*, *J* = 15.3 and 15.6 Hz, 1H, HC=CH), 7.29 and 7.19 (*s*, 1H, Ar-H), 7.20 and 7.07 (*d*, *J* = 8.1 and 8.0 Hz, 1H, Ar-H), 7.26 – 7.14 (*m*, 4H, Ar-H), 6.87 and 6.86 (*d*, *J* = 8.1 and 8.0 Hz, 1H, Ar-H), 3.86 and 3.83 (*s*, 3H, OCH_3), 3.04 (*s*, 12H, N-CH_3). ^{13}C NMR (75 MHz, DMSO- *d*$_6$) δ 166.57, 162.18, 149.27, 149.05, 148.18, 146.68, 142.88, 142.79, 140.93, 131.89, 128.83, 128.54, 126.72, 126.57, 122.44, 122.14, 117.40, 116.09, 115.56, 114.12, 112.37, 111.46, 56.10, 55.90, and 42.08. HRMS (ESI) *m/z*: Calcd for $C_{19}H_{22}N_3O_3$ $[M+H]^+$ 340.1661 found 340.1672 Calcd for $C_{19}H_{21}N_3NaO_3$ $[M+Na]^+$ 362.1481, found 362.1471.

3.1.17. (*E*)-*N*'-((*E*)-4-(diethylamino)benzylidene)-3-(4-hydroxy-3-methoxyphenyl)-acrylohydrazide (3o, PQM-220).

Yellow solid (yield 55%), m.p. 163 ºC, purity: 99.9 % (HPLC). IR (ATR): ν 3383, 3192, 2977, 1652, 1621, 1588 and 1358 cm^{-1}. ^{1}H NMR (300 MHz, DMSO- *d*$_6$) δ 11.27 and 11.06 (*s*, 1H, NH), 8.05 and 7.89 (*s*, 1H, N=CH), 7.56 and 7.48 (*d*, *J* = 15.4 and 15.8 Hz, 1H, HC=CH), 7.52 and 7.49 (*d*, *J* = 8.6 and 8.9 Hz, 2H, Ar-H), 7.37 and 6.49 (*d*, *J* = 15.9 and 15.8 Hz, 1H, HC=CH), 7.26 and 7.17 (*s*, 1H, Ar-H), 7.18 and 7.05 (*d*, *J* = 6.5 and 7.8 Hz, 1H, Ar-H), 6.84 and 6.81 (*d*, *J* = 6.5 and 7.8 Hz, 1H, Ar-H), 6.69 (*d*, *J* = 8.9 Hz, 1H, Ar-H), 3.85 and 3.85 (*s*, 3H, OCH_3), 3.38 (*dd*, *J* = 6.9 e 13.9 Hz, 8H, N-CH_2CH_3), 1.11 (*t*, *J* = 7.0 Hz, 12H, N-CH_2CH_3). ^{13}C NMR (75 MHz, DMSO- *d*$_6$) δ 166.22, 161.71, 129.02, 128.75, 126.56, 126.37, 122.29, 122.11, 117.31, 116.04, 114.22, 112.26, 111.35, 111.17, 56.03, 55.79, 44.00, and 12.72. HRMS (ESI) *m/z*: Calcd for $C_{21}H_{26}N_3O_3$ $[M+H]^+$ 368.1896, found 368.1963. Calcd for $C_{21}H_{25}N_3NaO_3$ $[M+Na]^+$ 390.1794, found 390.1783.

3.1.18. (*E*)-3-(4-hydroxy-3-methoxyphenyl)-*N*'-((*E*)-3,4,5-trimethoxybenzylidene)-acrylohydrazide (3p, PQM-221).

Light yellow solid (yield 52%), m.p. 205 ºC, purity: 99.9 % (HPLC). IR (ATR): ν 3337, 3222, 2942, 2838, 1652, 1590 and 1356 cm^{-1}. ^{1}H NMR (300 MHz, DMSO- d_6) δ 11.54 and 11.40 (*s*, 1H, NH), 9.53 (*s*, 2H, OH), 8.13 and 7.94 (*s*, 1H, N=CH), 7.56 and 7.51 (*d*, *J* = 15.3 and 15.7 Hz, 1H, HC=CH), 7.46 and 6.56 (*d*, *J* = 15.3 and 15.7 Hz, 1H, HC=CH), 7.34 and 7.18 (*s*, 1H, Ar-H), 7.09 and 7.07 (*d*, *J* = 7.8 and 8.9 Hz, 1H, Ar-H), 7.06 and 7.01 (*s*, 2H, Ar-H), 3.83 (*s*, 6H, OCH_3), 3.81 (*s*, 6H, OCH_3), 3.68 (*s*, 12H, OCH_3). ^{13}C NMR (75 MHz, DMSO- d_6) δ 166.92, 162.37, 153.63, 149.38, 149.21, 148.34, 146.60, 142.91, 142.75, 141.53, 139.58, 130.36, 126.84, 126.62, 123.63, 122.43, 117.21, 116.18, 114.28, 111.45, 110.84, 104.75, 104.45, 60.57, 56.41, and 55.71. HRMS (ESI) *m/z*: Calcd for $C_{20}H_{22}N_2NaO_6$ $[M+Na]^+$ 409.1376, found 409.1368.

3.1.19. (*E*)-*N*'-((*E*)-3,4-dimethoxybenzylidene)-3-(4-hydroxy-3-methoxyphenyl)-acrylohydrazide (3q, PQM-222).

Light yellow solid (yield 85%), m.p. 135 ºC, purity: 99.9 % (HPLC). IR (ATR): ν 3457, 3265, 3078, 2965, 1660, 1590 and 1368 cm^{-1}. ^{1}H NMR (300 MHz, DMSO- d_6) δ 11.43 and 11.27 (*s*, 1H, NH), 9.51 (*s*, 2H, OH), 8.12 and 7.95 (*s*, 1H, N=CH), 7.55 and 7.50 (*d*, *J* = 16.2 and 15.6 Hz, 1H, HC=CH), 7.44 and 6.50 (*d*, *J* = 16.2 and 15.6 Hz, 1H, HC=CH), 7.41 (*s*, H, Ar-H), 7.32 (*s*, 1H, Ar-H), 7.31 and 7.17 (*s*, 1H, Ar-H), 7.18 and 7.05 (*d*, *J* = 7.5 and 8.1 Hz, 1H, Ar-H), 7.12 (*d*, *J* = 8.3 Hz, 1H, Ar-H), 7.18 and 7.12 (*d*, *J* = 8.3 and 7.8 Hz, 2H, Ar-H)7.00 (*d*, *J* = 8.3 Hz, 1H, Ar-H), 6.98 (*d*, *J* = 8.0 Hz, 1H, Ar-H), 6.80 (*d*, *J* = 8.1 Hz, 2H, Ar-H), 3.83 (*s*, 6H, OCH_3), 3.81 (*s*, 3H, CH_3), 3.80 (*s*, 3H, CH_3), 3.78 (*s*, 6H, OCH_3). ^{13}C NMR (75 MHz, DMSO- d_6) δ 166.75, 162.20, 151.11, 150.83, 149.51, 149.33, 149.14, 148.34, 146.79, 143.06, 142.77, 141.24, 127.57, 126.90, 126.68, 123.29, 122.35, 122.18, 121.70, 117.37, 116.17, 116.05, 114.41, 111.93, 111.42, 111.29, 108.81, 108.73, 56.01, 55.86, and 55.66. HRMS (ESI) *m/z*: Calcd for $C_{19}H_{21}N_2O_5$ $[M+H]^+$ 357.1450, found 357.1444. Calcd for $C_{19}H_{20}N_2NaO_5$ $[M+Na]^+$ 379.1270, found 379.1263.

3.1.20. (*E*)-3-(4-hydroxy-3-methoxyphenyl)-*N*'-((*E*)-4-(piperidin-1-yl)benzylidene)-acrylohydrazide (3r, PQM-223).

Yellow solid (yield 75%), m.p. 120 ºC, purity: 99.9 % (HPLC). IR (ATR): ν 3160, 2948, 2837, 1654, 1579 and 1362 cm^{-1}. ^{1}H NMR (300 MHz, DMSO- d_6) δ 11.85 and 11.47 (*s*, 1H, NH), 8.27 and 8.07 (*s*, 1H, N=CH), 7.88 and 7.81 (*d*, *J* = 7.8 and 8.6 Hz, 2H, Ar-H), 7.80 – 7.67 (*m*, 2H, Ar-H), 7.61 and 7.54 (*d*, *J* = 15.8 and 15.9 Hz, 1H, HC=CH), 7.40 and 6.60 (*d*, *J* = 15.8 and 15.9 Hz, 1H, HC=CH), 7.31 and 7.20 (*s*, 1H, Ar-H), 7.21 and 7.08 (*d*, *J* = 7.0 and 7.8 Hz, 1H, Ar-H), 6.86 and 6.85 (*d*, *J* = 7.0 and 7.8 Hz, 1H, Ar-H), 3.86 and 3.82 (*s*, 3H, CH_3), 3.50 – 3.46 (*m*, 4H, $NHCH_2$), 1.97 – 1.89 (*m*, *J* = 7.0 Hz, 8H, $NHCH_2CH_2$), 1.69 – 1.61 (*m*, *J* = 9.2 Hz, 4H, CH_2). ^{13}C NMR (75 MHz, DMSO- d_6) δ

166.98, 162.49, 149.46, 149.27, 148.32, 145.33, 143.39, 141.93, 141.57, 128.74, 126.80, 126.62, 122.73, 122.39, 121.22, 120.89, 117.25, 116.21, 113.98, 112.58, 111.56, 56.22, 56.02, 54.55, 23.80 and 21.94. HRMS (ESI) *m/z*: Calcd for $C_{22}H_{26}N_3O_3$ $[M+H]^+$ 380.1974, found 380.1956.

3.1.21. (*E*)-3-(4-hydroxy-3-methoxyphenyl)-*N*'-((*E*)-4-(pyrrolidin-1-yl)benzylidene)-acrylohydrazide (3s, PQM-224).

Green solid (yield 44%), m.p. 245 ºC, purity: 99.7 % (HPLC). IR (ATR): ν 3193, 3038, 2821, 1645, 1614, 1581 and 1395 cm^{-1}. ^1H NMR (300 MHz, DMSO- d_6) δ 11.24 and 11.05 (*s*, 1H, NH), 9.49 (*s*, 2H, OH), 8.04 and 7.89 (*s*, 1H, N=CH), 7.52 and 7.50 (*d*, *J* = 8.5 Hz, 2H, Ar-H), 7.47 and 7.42 (*d*, *J* = 15.9 and 15.8 Hz, 1H, HC=CH), 7.37 and 6.48 (*d*, *J* = 15.9 and 15.8 Hz, 1H, HC=CH), 7.26 and 7.16 (*s*, 1H, Ar-H), 7.16 and 7.04 (*d*, *J* = 7.4 and 7.6 Hz, 1H, Ar-H), 6.83 and 6.80 (*d*, *J* = 7.4 and 7.6 Hz, 2H, Ar-H), 6.55 (*d*, *J* = 8.5 Hz, 4H, Ar-H), 3.84 and 3.81 (*s*, 3H,OCH_3), 3.26 (*s*, 8H, NCH_2 CH_2), 1.94 (*s*, 8H, NCH_2CH_2). ^{13}C NMR (75 MHz, DMSO- d_6) δ 166.36, 161.84, 149.22, 149.01, 148.30, 147.64, 144.27, 142.49, 140.68, 129.01, 128.75, 127.01, 126.80, 122.41, 122.22, 121.46, 117.66, 116.17, 114.62, 112.40, 112.01, 111.34, 56.20, 55.98, 47.69 and 25.42. HRMS (ESI) *m/z*: Calcd for $C_{21}H_{24}N_3O_3$ $[M+H]^+$ 366.1818, found 366.1813.

3.1.22. (*E*)-3-(4-hydroxy-3-methoxyphenyl)-*N*'-((*E*)-4-morpholinobenzylidene)-acrylohydrazide (3t, PQM-225).

Light pink solid (yield 47%), m.p. 225 ºC, purity: 99.9 % (HPLC). IR (ATR): ν 3350, 3173, 3024, 2882, 1674, 1628, 1601 and 1315 cm^{-1}. ^1H NMR (300 MHz, DMSO- d_6) δ 11.51 and 11.21 (*s*, 1H, NH), 8.10 and 7.93 (*s*, 1H, N=CH),), 7.60 and 7.56 (*d*, *J* = 8.9 Hz, 2H, Ar-H), 7.56 and 7.48 (*d*, *J* = 15.7 Hz, 1H, HC=CH), 7.36 and 6.52 (*d*, *J* = 15.7 Hz, 1H, HC=CH), 7.26 and 7.17 (*d*, *J* = 1.6 Hz, 1H, Ar-H), 7.18 and 7.05 (*d*, *J* = 1.6; 7.6 and 1.6; 8.3 Hz, 1H, Ar-H), 6.99 (*d*, *J* = 8.9 Hz, 2H, Ar-H), 6.85 and 6.81 (*d*, *J* = 7.6 and 8.3 Hz, 1H, Ar-H), 3.83 and 3.80 (*s*, 3H, OCH_3), 3.76 – 3.69 (*m*, 4H, OCH_2), 3.23 – 3.15 (*m*, 4H, NCH_2). ^{13}C NMR (75 MHz, DMSO- d_6) δ 166.50, 162.10, 152.39, 152.19, 149.28, 149.07, 148.28, 146.82, 143.52, 142.84, 141.23, 128.50, 126.89, 126.69, 126.34, 122.51, 122.32, 117.45, 116.14, 115.10, 114.94, 114.34, 112.39, 111.32, 63.37, 56.16, 55.95, and 48.02. HRMS (ESI) *m/z*: Calcd for $C_{21}H_{24}N_3O_4$ $[M+H]^+$ 382.1767, found 382.1751.

3.1.23. (*E*)-*N*'-((*E*)-4-(1H-imidazol-1-yl)benzylidene)-3-(4-hydroxy-3-methoxyphenyl)-acrylohydrazide (3u, PQM-226).

Yellow solid (yield 87%), m.p. 262 ºC, purity: 99.9 % (HPLC). IR (ATR): ν 3138, 3023, 2734, 1668, 1634, 1593 and 1360 cm^{-1}. ^1H NMR (300 MHz, DMSO- d_6) δ 12.12 and 11.57 (*s*, 1H, NH), 9.80 (*s*, 2H, OH), 8.37 and 8.14 (*s*, 1H, N=CH), 8.34 (*t*, *J* = 1.7 Hz, 2H, NCH=N), 8.00 (*d*, *J* = 8.3 Hz, 2H, NCH=CH), 7.96 – 7.90 (*m*, 10H, Ar-H), 7.88 (*d*, *J* = 2.1 Hz, 2H, NCH=CH), 7.60 and 7.53 (*d*, *J* = 15.9 and 15.7 Hz, 1H, HC=CH), 7.41 and 6.65 (*d*, *J* = 15.9 and 15.7 Hz, 1H, HC=CH), 7.30 and 7.18 (*s*,

1H, Ar-H), 7.22 and 7.06 (*d*, *J* = 7.8 and 7.9 Hz, 1H, Ar-H), 6.87 and 6.84 (*d*, *J* = 7.8 and 7.9 Hz, 1H, Ar-H), 3.84 and 3.80 (*s*, 3H, OCH$_3$). ^{13}C NMR (75 MHz, DMSO- *d*$_6$) δ 167.09, 162.67, 149.54, 149.35, 148.32, 144.73, 143.57, 141.70, 141.57, 135.99, 135.83, 135.00, 128.77, 126.76, 126.58, 122.71, 122.40, 121.53, 121.07, 117.24, 116.22, 113.90, 112.63, 111.63, 56.23, and 56.03. HRMS (ESI) *m/z*: Calcd for $C_{20}H_{19}N_4O_3$ $[M+H]^+$ 363.1457, found 363.0936.

3.1.24. (*E*)-3-(4-hydroxy-3-methoxyphenyl)-*N*'-((*E*)-4-(pyrimidin-5-yl)benzylidene)-acrylohydrazide (3v, PQM-227).

Yellow solid (yield 78%), m.p. 225 ºC, purity: 99.9 % (HPLC). IR (ATR): ν 3512, 3208, 3055, 1669, 1651, 1591 and 1397 cm^{-1}. ^{1}H NMR (300 MHz, DMSO- *d*$_6$) δ 11.86 and 11.50 (*s*, 1H, NH), 9.20 (*s*, 2H, OH), 8.30 and 8.10 (*s*, 1H, N=CH), 7.81 and 7.70 (*d*, *J* = 7.8 and 7.7 Hz, 2H, Ar-H), 7.90 (*s*, 2H, Ar-H), 7.85 (*d*, *J* = 8.4 Hz, 8H, Ar-H), 7.60 and 7.53 (*d*, *J* = 15.9 and 15.6 Hz, 1H, HC=CH), 7.41 and 6.58 (*d*, *J* = 15.9 and 15.6 Hz, 1H, HC=CH), 7.30 and 7.18 (*s*, 1H, Ar-H), 7.21 and 7.07 (*d*, *J* = 7.8 and 1.9 Hz, 1H, Ar-H), 6.85 and 6.82 (*d*, *J* = 7.8 and 1.9 Hz, 1H, Ar-H), 3.84 and 3.80 (*s*, 3H, OCH$_3$). ^{13}C NMR (75 MHz, DMSO- *d*$_6$) δ 167.01, 162.51, 157.73, 155.16, 149.45, 149.28, 148.31, 145.64, 143.42, 142.40, 141.65, 135.47, 135.28, 135.07, 133.05, 128.24, 127.37, 126.81, 126.60, 122.63, 122.42, 117.21, 116.20, 113.98, 112.65, 111.68, 56.23 and 55.99. HRMS (ESI) *m/z*: Calcd for $C_{21}H_{19}N_4O_3$ $[M+H]^+$ 375.1457, found 375.1443. Calcd for $C_{21}H_{18}N_4NaO_3$ $[M+Na]^+$ 397.1277, found 397.1262.

3.1.25. (*E*)-*N*'-((*E*)-benzo[d][1,3]dioxol-5-ylmethylene)-3-(4-hydroxy-3-methoxyphenyl)-acrylohydrazide (3w, PQM-228).

Yellow solid (yield 61%), m.p. 217 ºC, purity: 99.9 % (HPLC). IR (ATR): ν 3433, 3240, 3066, 2903, 1666, 1623, 1591, 1373 and 1029 cm^{-1}. ^{1}H NMR (300 MHz, DMSO- *d*$_6$) δ 11.46 and 11.23 (*s*, 1H, NH), 9.51 (*s*, 2H, OH), 8.11 and 7.94 (*s*, 1H, N=CH), 7.56 and 7.50 (*d*, *J* = 15.7 and 15.6 Hz, 1H, HC=CH), 7.37 and 6.48 (*d*, *J* = 15.7 and 15.6 Hz, 1H, HC=CH), 7.42 and 7.26 (*s*, 1H, Ar-H), 7.27 and 7.16 (*s*, 1H, Ar-H), 7.21 and 7.05 (*d*, *J* = 7.9 and 8.1 Hz, 1H, Ar-H), 7.15 and 7.12 (*d*, *J* = 8.0 and 7.9 Hz, 1H, Ar-H), 6.96 (*d*, *J* = 8.0 Hz, 2H, Ar-H), 6.95 (*d*, *J* = 7.9 Hz, 1H, Ar-H), 6.82 and 6.80 (*d*, *J* = 7.9 and 8.1 Hz, 1H, Ar-H), 6.06 (*s*, 4H, OCH$_2$O), 3.83 and 3.80 (*s*, 3H, OCH$_3$). ^{13}C NMR (75 MHz, DMSO- *d*$_6$) δ 166.80, 162.26, 149.44, 149.32, 149.17, 148.43, 148.31, 146.38, 143.07, 141.34, 129.29, 126.91, 126.66, 123.67, 123.50, 122.58, 122.37, 117.28, 116.19, 114.25, 112.69, 111.43, 108.88, 105.62, 101.97, 56.21 and 55.99. HRMS (ESI) *m/z*: Calcd for $C_{18}H_{16}N_2NaO_5$ $[M+Na]^+$ 363.0957, found 363.1467.

3.1.26. (*E*)-*N*'-((*E*)-4-hydroxybenzylidene)-3-(4-methoxyphenyl)acrylohydrazide (4a, PQM-196).

Light yellow solid (yield 76%), m.p. 254 ºC, purity: 99.9 % (HPLC). IR (ATR): ν 3250, 3012, 2898, 1636, 1602, 1562, 1458, 1365 and 1022 cm^{-1}. ^1H NMR (300 MHz, DMSO-*d6*) δ 11.41 and 11.21 (*s*, 1H, N-NH), 9.92 (*s*, 1H, OH), 8.12 and 7.95 (*s*, 1H, N=CH), 7.61-7.51 (*m*, 4H, Ar-H), 7.43 (*d*, *J* = 15.67 Hz, 1H, HC=CH), 6.99 (*d*, J = 8.17 Hz, 2H, Ar-H), 6.83 (*d*, J = 8.08 Hz, 2H, Ar-H), 6.54 (*d*, *J* = 15.67 Hz, 1H, HC=CH) and 3.79 (*s*, 3H, CH_3). ^{13}C NMR (75 MHz, DMSO-*d_6*) δ 166.5, 162.0, 161.1, 147.1, 143.7, 130.3, 129.8, 129.3, 129.0, 125.8, 116.2, 114.9, and 55.7. HRMS (ESI) *m/z*: Calcd for $C_{17}H_{17}N_2O_3$ $[M+H]^+$ 297.1239, found 297.1231.

3.1.27. *N*'-(3,5-dihydroxybenzylidene)-3-(4-methoxyphenyl)acrylohydrazide (4b, PQM-197).

Beige solid (yield 22%). m.p. 211 ºC, purity: 95.0 % (HPLC). IR (ATR): *v* 3252, 3061, 2843, 1662, 1589, 1551, 1465, 1304, 1289 and 1043. ^1H NMR (300 MHz, DMSO-*d6*) δ 11.49 and 11.30 (*s*, 1H, N-NH), 9.44 (*s*, 4H, OH), 8.02 and 7.85 (*s*, 1H, N=CH), 7.61-7.51 (*m*, 4H, Ar-H), 7.37 (*d*, *J* = 15.97 Hz, 1H, HC=CH), 7.06-6.96 (*m*, 4H, Ar-H), 6.61-6.57 (*m,* 4H, Ar-H), 6.53 (*d*, *J* = 15.97 Hz, 1H, HC=CH), 6.26 (*s*, 2H, Ar-H) and 3.80 (*s*, 6H, CH_3). ^{13}C NMR (75 MHz, DMSO-*d_6*) δ 166.2, 160.7, 158.7, 146.6, 143.3, 136.1, 129.4, 127.3, 117.7, 114.5, 105.2, 104.4, and 55.3. HRMS (ESI) *m/z*: Calcd for $C_{17}H_{17}N_2O_4$ $[M+H]^+$: 313.1188, found 313.1193.

3.1.28. *N*'-(4-methoxybenzylidene)-3-(4-methoxyphenyl)acrylohydrazide (4c, PQM-198).

Withe solid (yield 44%), m.p. 278 ºC, purity: 99.9 % (HPLC). IR (ATR): *v* 3007, 2929, 1647, 1600, 1508, 1421, 1253 e 1028. ^1H NMR (300 MHz, DMSO-*d6*) δ 11.46 and 11.30 (*s*, 1H, N-NH), 8.18 and 8.00 (*s*, 1H, N=CH), 7.74-7.65 and 7.62-7.51 (*m*, 4H, Ar-H), 7.45 (*d*, *J* = 15.90 Hz, 1H, HC=CH), 7.01 (*d*, J = 8.59 Hz, 8H, Ar-H), 6.55 (*d*, *J* = 15.90 Hz, 1H, HC=CH) and 3.80 (*s*, 12H, CH_3). ^{13}C NMR (75 MHz, DMSO-*d_6*) δ 166.1, 160.8, 160.61, 146.2, 142.7, 129.9, 129.4, 128.7, 128.4, 117.8, 114.5, 114.3, and 55.3. HRMS (ESI) *m/z*: Calcd for $C_{18}H_{19}N_2O_3$ $[M+H]^+$: 311.1396, found 311.1385.

3.1.29. *N*'-(3,5-dimethoxybenzylidene)-3-(4-methoxyphenyl)acrylohydrazide (4d, PQM-199).

Light yellow solid (yield 74%), m.p. 228 ºC, purity: 99.9 % (HPLC). IR (ATR): *v* 3166, 3139, 3045, 2933, 2834, 1663, 1602, 1582, 1419, 1382, 1053. ^1H NMR (300 MHz, pyridine-*d5*) δ 12.62 and 12.60 (*s*, 1H, N-NH), 8.65 and 8.41 (*s*, 1H, N=CH), 8.23 and 8.03(*d*, *J* = 15.60 e 15.91 Hz, 1H, HC=CH), 7.72 (*d*, *J* = 8.48 Hz, 2H, Ar-H), 7.52 (*d*, *J* = 8.42 Hz, 2H, Ar-H), 7,29 (*dd*, *J* = 1.48, 9.36 Hz, 4H, Ar-H), 7.03-6.88 (*m*, 6H, Ar-H), 6.78 and 6.72 (*s*, 1H, Ar-H), 3.77 (*s*, 9H, CH_3), 3.68 (*s*, 3H, CH_3), 3,65 (*s*, 3H, CH_3) and 3,63 (*s*, 3H, CH_3). ^{13}C NMR (75 MHz, pyridine-*d_5*) δ 168.2, 163.8, 162.1, 162.0, 147.4, 143.4, 143.3, 142.3, 137.8, 130.8, 130.3, 129.0, 128.6, 118.6, 116.2, 115.3, 106.1, 103.8, 102.9, and 55.8. HRMS (ESI) *m/z*: Calcd for $C_{19}H_{21}N_2O_4$ $[M+H]^+$: 341.1501, found 341.1482.

3.1.30. *N*'-(4-hydroxy-3-methoxybenzylidene)-3-(4-methoxyfenyl)acrylohydrazide (4e, PQM-200).

Light yellow solid (yield 70%), m.p. 263 ºC, purity: 99.9 % (HPLC). IR (ATR): *v* 3274, 2997, 2839, 1651, 1600, 1511, 1442, 1274 e 1017. ^{1}H NMR (300 MHz, DMSO-*d6*) δ 11.63 and 11.27 (*s*, 1H, N-NH), 8.12 and 7.92 (*s*, 1H, N=CH), 7,67 (*d*, *J* = 8.58 Hz, 1H, Ar-H), 7.60-7.51 (*m*, 4H, Ar-H), 7.41 (*d*, *J* = 15.72 Hz, 1H, HC=CH), 7.28 (*dd*, *J* = 1.60, 8.07 Hz, 2H, Ar-H), 7.08-6.92 (*m*, 8H, Ar-H), 6.60 (*d*, *J* = 15.72 Hz, 1H, HC=CH) and 3.80 (*s*, 6H, CH_3). ^{13}C NMR (75 MHz, DMSO-d_6) δ 166.5, 162.0, 161.0, 150.2, 147.3, 143.5, 136.1, 142.0, 140.3, 129.8, 120.7, 118.4, 114.9, 112.3, 56.0, and 55.8. HRMS (ESI) *m/z*: Calcd for $C_{18}H_{19}N_2O_4$ $[M+H]^+$: 327.1345, found 327.1355.

3.2. Pharmacological Experiments

3.2.1. Determination of DPPH Scavenging Ability

The ability of compounds to sequester DPPH free radicals was evaluated according to the method described by Gontijo and co-workers with modifications [51]. The compounds were evaluated at concentrations of 100, 50, 25, and 12.5μM. A 4 mL aliquot of the sample was added to 1 mL of the DPPH solution (0.5 mM in ethanol). The solution was vortexed and after 30 minutes the absorbance was measured at 517 nm. Each solution was analyzed in triplicate and the mean values were plotted to obtain the EC_{50}. Trolox and ascorbic acid were used as standards. The sequestering capacity of radicals was represented as inhibition percentage according to the equation: % sequestering capacity = [(control absorbance - sample absorbance) / control absorbance)] × 100.

3.2.2. Evaluation of Chelating Capacity of Biometals Cu^{+2}, Fe^{+2}, Fe^{+3}, and Zn^{+2}

The ability of the compounds to chelate biometals, such as Cu^{+2}, Fe^{+2}, Fe^{+3}, and Zn^{+2}, was performed using the UV-vis spectrophotometer (Shimadzu) following the methodology described by Chen et al. [52] Two 20 μM solutions of the compounds were prepared in methanol and one without metals and the other in the presence of 20 μM $CuSO_4$, $FeSO_4$, $FeCl_3$ and $ZnCl_2$. The spectra were obtained at room temperature in a quartz cuvette.

3.2.3. Cell Cultures and Preparation of Compound Solutions

Human neuronal SH-SY5Y cells were routinely grown in Dulbecco's modified Eagle' Medium (DMEM) supplemented with 10% fetal bovine serum, 2 mmol/l-glutamine, 50 U/mL penicillin and 50 mg/mL streptomycin at 37°C in a humidified incubator with 5% CO_2. For all experiments, the SH-SY5Y cells were used below passage 12 to avoid phenotype changes and cellular senescence. Stock solutions of the compounds were prepared in dimethyl sulfoxide (DMSO) at 20 mM. The stock

solutions were further diluted in a complete medium to obtain the desired concentrations of compounds in a maximum of 0.1% DMSO.

3.2.4. Determination of Neurotoxicity

Neuronal viability in terms of mitochondrial activity was evaluated with the 3-(4,5-dimethyl-2-thiazolyl)-2,5-diphenyl-2H-tetrazolium bromide (MTT) assay, as previously described [53]. Briefly, SH-SY5Y cells were seeded in 96-well plates at 2 x 10^4 cells/well, incubated for 24 h, and subsequently treated with various concentrations of compounds (2.5 - 80 µM) for 24 h at 37°C in 5% CO_2. The treatment medium was then replaced with MTT (5 mg/mL) in phosphate-buffered saline (PBS) for 2 h at 37°C in 5% CO_2. After washing with PBS, the formazan crystals were dissolved with isopropanol. The amount of formazan was measured (570 nm, reference filter 690 nm) using a multilabel plate reader (VICTOR™ X3, PerkinElmer, Waltham, MA, USA). The neurotoxicity is expressed as the concentration of the compound resulting in 50% inhibition of cell viability.

3.2.5. Determination of Intracellular ROS Formation

ROS formation was determined using the fluorescent probe 2'-7'-dichlorodihydrofluorescein diacetate (DCFH-DA), as previously reported [54]. Briefly, SH-SY5Y cells were seeded in 96-well plates at 3 x 10^4 cells/well and incubated for 24 h at 37°C in 5% CO_2. Subsequently, the cell culture medium was removed, and 100 mL of DCFH-DA (10 mg/mL) was added to each well. After 30 min of incubation at room temperature, the DCFHDA solution was replaced with the solutions of the compounds (10 µM) and either t-BOOH (100 µM) or $FeSO_4/H_2O_2$ (25 µM/100 µM). In parallel, the SH-SY5Y cells were also treated with compounds (10 µM) for 24 h before the treatment with t-BOOH. The ROS formation was measured (excitation at 485 nm and emission at 535 nm) using a multilabel plate reader (VICTOR™X3). The values are expressed as % inhibition of ROS formation induced by t-BOOH or $FeSO_4/H_2O_2$.

3.2.6. Determination of Intracellular GSH Levels

Cellular GSH levels were determined by the monochlorobimane (MCB) assay in 96-well plates as previously reported with minor modification [55]. Briefly, SH-SY5Y cells were seeded in 96-well plates at 2 x 10^4 cells/well, incubated for 24 h, and subsequently treated with 2.5 µM of compound for 24 h at 37°C in 5% CO_2. The treatment medium was then replaced with MCB (50 mM) in PBS for 30 min at 37°C in 5% CO_2. The amount of GSH was measured (excitation at 360 nm and emission at 465 nm) using a multilabel plate reader (VICTOR™ X3, PerkinElmer, Waltham, MA, USA). The values are expressed as a fold increase.

3.2.7. Nuclear Extraction and Nrf2 Binding Activity Assay

Nuclear extraction and Nrf2 binding activity assay were performed using the Nuclear Extract and TransAM Nrf2 kits (Active Motif, Carlsbad, CA, USA), respectively, according to the manufacturer's guidelines. Protein concentration in samples was measured using the Bio-Rad Protein Assay Dye reagent. Briefly, SH-SY5Y cells were seeded in culture dishes (size 60 mm) at 2 x 10^6 cells/dish, incubated for 24 h, and subsequently treated with 2.5 μM of compound for 3 h at 37°C in 5% CO_2. At the end of treatment, 20 μg of nuclear extract was evaluated by TransAM Nrf2 Kit. The values are expressed as a fold increase.

3.2.8. Determination of Neuroprotective Activity

Neuronal SH-SY5Y cells were seeded in a 96-well plate at 3 × 10^4 cells/well, incubated for 24 h, and subsequently treated with compounds (2.5 μM) and 6-hydroxydopamine (6-OHDA, 100 μM) for 2 h and starved in complete medium for 22 h. In parallel, the SH-SY5Y cells were also treated with compounds (2.5 μM) for 24 h before the treatment with 6-OHDA. The neuroprotective activity was measured by using the MTT assay as previously described [41]. Data are expressed as a percentage of inhibition of neurotoxicity induced by 6-OHDA.

3.2.9. Detection of α-Synuclein Aggregation

TagGFP2-α-synuclein SH-SY5Y cells were seeded in a 96-well plate at 2 × 10^4 cells/well, incubated for 24 h, and subsequently treated with compounds (2.5 μM) and 6-OHDA (100 μM) for 2 h at 37 °C in 5% CO_2. At the end of incubation, the aggregation of α-synuclein was detected using an inverted fluorescent microscope (Eclipse Ti-E, Nikon Instruments Spa, Florence, Italy) as previously described [41]. The intensity of fluorescence was directly proportional to the aggregation of α-synuclein. Data are expressed as relative fluorescence units (RFU).

3.2.10. Determination of Gene Expression

NQO1, GSS, iNOS, IL-1β, and TNF-α gene expression was determined by Real-Time PCR as previously reported [41,56]. Neuronal SH-SY5Y cells were seeded in 100 mm dishes at 2.5 × 10^6 cells/dish, incubated for 24 h, and then treated with compounds (2.5 μM) for 24 h at 37 °C and in 5% CO_2; microglial THP-1 cells were seeded in 60 mm dishes at 2.5 × 10^6 cells/dish, incubated for 24 h with PMA (10 μg/mL) and subsequently, treated for 24 h with compounds (10 μM) and LPS (1 μg/mL).

After the different treatments, total RNA was extracted by the PureLink RNA Mini Kit (Life Technologies, Carlsbad, CA, USA) according to the manufacturer's guidelines. A total of 1 μg of RNA was used to synthesize cDNA using the SuperScript VILO MasterMix (Invitrogen, Carlsbad, CA, USA). Quantitative Real-Time PCR was carried out using SYBR Select Master Mix (Invitrogen), and

relative normalized expression was calculated by comparing the cycle threshold (Ct) of the target gene to that of the reference genes beta-2 microglobulin (B2M) and TATA-box binding protein (TBP, Life Technologies) for SH-SY5Y cells and β-Actin and glyceraldehyde-3-phosphate dehydrogenase protein (GAPDH, Life Technologies) for THP-1 cells. All reactions had three technical replicates, and each condition had three biological replicates. Relative quantification was calculated according to the ΔΔCt method (2−ΔΔCt) with untreated cells as control. Primer sequences used in this study are listed in Table 3.

Table 3. Neurotoxicity and in silico ADME properties of cinnamic acid hybrids.

SH-SY5Y cells		
Gene[a]	Forward	Reverse
NQO1	GGGATCCACGGGGACATGA	ATTTGAATTCGGGCGTCTGC
GSS	CACAAGCAAGTCCTAAAAGAG	GATGGTGTTGATTTCGATCTGT
B2M	CTTTCCATTCTCTGCTGGATGACG	GCGGGCATTCCTGAAGCTGACAGCA
TBP	CACATCACAGCTCCCCACCA	TGCACAGGAGCCAAGAGTGAA
THP-1 cells		
Gene[b]	Forward	Reverse
iNOS	TGAACTACGTCCTGTCCCCT	CTCTTCTCTTGGGTCTCCGC
IL-1β	TGATGGCTTATTACAGTGGCAATG	GTAGTGGTGGTCGGAGATTCG
TNF-α	ATCTTCTCGAACCCCGAGTG	GGGTTTGCTACAACATGGGC
B-actin	GCGAGAAGATGACCCAGATC	GGATAGCACAGCCTGGATAG
GAPDH	GGTCGGAGTCAACGGATTTG	GGAAGATGGTGATGGGATTTC

[a]NQO1, NAD(P)H:quinone oxidoreductase 1; GSS, glutathione synthetase; B2M, beta-2 microglobulin; TBP, TATA-box binding protein. [b]iNOS, Inducible nitric oxide synthase; IL-1β, Interleukin 1 beta; TNF-α, Tumour Necrosis Factor-alpha; GAPDH, glyceraldehyde-3-phosphate dehydrogenase protein.

3.2.11. Human Monoamine Oxidases Inhibition Assays

Human monoamine oxidase inhibition assays were carried out with a fluorescence-based method [57], using kynuramine as a nonselective MAO A and MAO B substrate. Human recombinant MAO A and MAO B (microsomes from baculovirus-infected insect cells; Sigma-Aldrich) were used. Samples were preincubated for 20 min at 37 °C before adding MAO solutions, then incubated for an

additional 30 min. Fluorescence was recorded at excitation/emission wavelengths of 320/400 nm (20 nm slit width for excitation, 30 nm slit width for emission) in a 96-well microplate fluorescence reader (Tecan Infinite M100 Pro). Inhibitory activities were determined employing nonlinear regressions performed with GraphPad Prism 5.0 software and are expressed as percentages of inhibition at 10 μM. Results are the mean of three independent experiments.

3.2.12. Evaluation of Cytotoxicity in VERO Cells Culture

Cytotoxicity evaluation of the substances was performed using the MTT method (Sigma-Aldrich, USA). VERO cells were cultured in DMEM medium (Vitrocell Embriolife, Brazil) containing 5% FBS (Vitrocell Embriolife, Brazil) and penicillin and streptomycin antibiotics (Vitrocell Embriolife, Brazil) at a concentration of $1x10^4$ cells per well in 96-well plates. (TPP, Switzerland). After 24 hours of incubation at 37 °C and 5% CO_2, the cells were treated in triplicate with various concentrations (500-0.48 μg/mL) of the test substances, serially diluted. Cells were incubated at 37 °C at 5% CO_2 for 48 hours. Subsequently, 10 μl MTT (5 mg/ml) was added to each well, and the cells were incubated at 37 °C and 5% CO_2 for 4 hours. Then the medium was removed and 100 μL of DMSO was added to each well for the solubilization of formazan crystals. The absorbance of each well was measured on the Anthos Zenyth 200rt microplate reader (Biochrom, UK) at 570 nm. The cytotoxicity of the test substances was obtained by the following formula: [(A-B) / Ax100] where A represents the absorbance of the control cells and B the absorbance of the cells treated with the different concentrations of the substances. Cytotoxic concentration in 50% of cells was determined by linear regression.

4. Conclusion

A novel series of 28 *N*-aryl-cinnamoyl-hydrazone derivatives, with a hybrid curcumin-resveratrol-based structural architecture, was synthesized with overall yields of 17-78%. Pharmacological evaluation of compounds **3a-3w** and **4a-4e** led to the identification of derivatives **3b (PQM-161)** and **3e (PQM-164)**, which showed a highlighted complete antioxidant profile, acting directly on the stabilization of DPPH free radicals (**3b**, EC_{50}= 19.98 μM and **3e**, EC_{50}= 0.93 μM) and indirectly by modulating intracellular inhibition of *t*-BOOH-induced ROS formation in neuronal cells (**3b**, IC_{50} = 0.71 μM and **3e**, IC_{50}= 0.51 μM). Our results suggested that the decrease in both ROS production and neurotoxicity would be due to the induction in GSH production, resulting from the treatment of neuronal cells with the tested compounds at different time intervals. Additional studies confirmed this mechanism of action, making it evident that the increase in GSH levels is, in fact, due to the activation of Nrf2, a property identified for both compounds and confirmed by molecular

docking and gene expression studies. In addition, the effect of compound **3e (PQM-164)** on α-synuclein protein accumulation was identified. Although this compound did not inhibit α-syn accumulation, it was able to promote the clearance of protein deposits, reducing the concentration of insoluble α-syn in treated cells to practically basal levels. Finally, the anti-inflammatory activity of **3e (PQM-164)** was evidenced, as being capable of significantly decreasing in gene expression of iNOS, IL-1β, and TNF-α. Finally, it is noteworthy that none of the tested compounds elicited relevant cytotoxicity and neurotoxicity, with adequate *in-silico* prediction of druggability and pharmacokinetic parameters. Taking together, these results highlighted compound **3e (PQM-164)** as a promising multifunctional drug candidate prototype suitable for the development addressed to the treatment of Parkinson's disease.

Acknowledgments

The authors are grateful to the National Institute of Science and Technology of Drugs and Medicines Program (INCT-INOFAR, CNPq, Brazil, #465249/2014-0), and to the Brazilian Agencies FAPEMIG (Brazil, # CEX-PPM-00241-15, #APQ-CEX 00518-17), CNPq (Brazil, #454088/2014-0, #400271/2014-1, #406739-2018-8, #303804-2020-3) for financial support. The authors are also grateful for the fellowships granted by CAPES (code number 001) to MFS and CJCO.

References

[1] M.T. Lin, M.F. Beal, Mitochondrial dysfunction and oxidative stress in neurodegenerative diseases, Nature. 443 (2006) 787–795. https://doi.org/10.1038/nature05292.

[2] J.T. Coyle, P. Puttfarcken, Oxidative stress, glutamate and neurodegenerative disorders., Science (80-.). 262 (1993) 689–95.

[3] E.M. Rocha, B. De Miranda, L.H. Sanders, Alpha-synuclein: Pathology, mitochondrial dysfunction and neuroinflammation in Parkinson's disease, Neurobiol. Dis. 109 (2018) 249–257. https://doi.org/10.1016/j.nbd.2017.04.004.

[4] C. Castillo-Rangel, G. Marin, K.A. Hernández-Contreras, M.M. Vichi-Ramírez, C. Zarate-Calderon, O. Torres-Pineda, D.L. Diaz-Chiguer, D. De la Mora González, E. Gómez Apo, J.A. Teco-Cortes, F. de M. Santos-Paez, M. de los Á. Coello-Torres, M. Baldoncini, G. Reyes Soto, G.E. Aranda-Abreu, L.I. García, Neuroinflammation in Parkinson's Disease: From Gene to Clinic: A Systematic Review, Int. J. Mol. Sci. 24 (2023) 5792. https://doi.org/10.3390/ijms24065792.

[5] B.G. Trist, D.J. Hare, K.L. Double, Oxidative stress in the aging substantia nigra and the etiology of Parkinson's disease, Aging Cell. 18 (2019). https://doi.org/10.1111/acel.13031.

[6] P.A. Dionísio, J.D. Amaral, C.M.P. Rodrigues, Oxidative stress and regulated cell death in Parkinson's disease, Ageing Res. Rev. 67 (2021) 101263. https://doi.org/10.1016/j.arr.2021.101263.

[7] P. Huot, Monoamine oxidase A inhibition and Parkinson's disease, Neurodegener. Dis. Manag. 10 (2020) 335–337. https://doi.org/10.2217/nmt-2020-0043.

[8] M. Valko, D. Leibfritz, J. Moncol, M.T.D. Cronin, M. Mazur, J. Telser, Free radicals and antioxidants in normal physiological functions and human disease, Int. J. Biochem. Cell Biol. 39 (2007) 44–84. https://doi.org/10.1016/j.biocel.2006.07.001.

[9] M. Salazar, A.I. Rojo, D. Velasco, R.M. De Sagarra, A. Cuadrado, Glycogen synthase kinase-3β inhibits the xenobiotic and antioxidant cell response by direct phosphorylation and nuclear exclusion of the transcription factor Nrf2, J. Biol. Chem. 281 (2006) 14841–14851. https://doi.org/10.1074/jbc.M513737200.

[10] G.J. McBean, M.G. López, F.K. Wallner, Redox-based therapeutics in neurodegenerative disease, Br. J. Pharmacol. 174 (2017) 1750–1770. https://doi.org/10.1111/bph.13551.

[11] Y. Izumi, H. Kataoka, Y. Inose, A. Akaike, Y. Koyama, T. Kume, Neuroprotective effect of an Nrf2-ARE activator identified from a chemical library on dopaminergic neurons, Eur. J. Pharmacol. 818 (2018) 470–479. https://doi.org/10.1016/j.ejphar.2017.11.023.

[12] A. Cuadrado, A.I. Rojo, G. Wells, J.D. Hayes, S.P. Cousin, W.L. Rumsey, O.C. Attucks, S. Franklin, A.-L. Levonen, T.W. Kensler, A.T. Dinkova-Kostova, Therapeutic targeting of the NRF2 and KEAP1 partnership in chronic diseases, Nat. Rev. Drug Discov. 18 (2019) 295–317. https://doi.org/10.1038/s41573-018-0008-x.

[13] J.A. Johnson, D.A. Johnson, A.D. Kraft, M.J. Calkins, R.J. Jakel, M.R. Vargas, P. Chen, The Nrf2–ARE Pathway: An indicator and modulator of oxidative stress in neurodegeneration, Ann. N. Y. Acad. Sci. 1147 (2008) 61–69. https://doi.org/10.1196/annals.1427.036.

[14] M. de Freitas Silva, L. Pruccoli, F. Morroni, G. Sita, F. Seghetti, C. Viegas, A. Tarozzi, The Keap1/Nrf2-ARE Pathway as a Pharmacological Target for Chalcones, Molecules. 23 (2018) 1803. https://doi.org/10.3390/molecules23071803.

[15] X. Zhao, J. Wang, S. Hu, R. Wang, Y. Mao, J. Xie, Neuroprotective effect of resveratrol on rotenone-treated C57BL/6 mice, Neuroreport. 28 (2017) 498–505. https://doi.org/10.1097/WNR.0000000000000789.

[16] L. Chen, J. Xie, Dopamine in Parkinson's Disease: Precise Supplementation with Motor Planning, Neurosci. Bull. 34 (2018) 873–874. https://doi.org/10.1007/s12264-018-0245-3.

[17] W. Dauer, S. Przedborski, Parkinson's Disease: Mechanisms and Models, Neuron. 39 (2003) 889–909.

[18] D. Gupta, A. Julka, S. Jain, T. Aggarwal, A. Khanna, N. Arunkumar, V.H.C. de Albuquerque, Optimized Cuttlefish Algorithm for Diagnosis of Parkinson's Disease, Cogn. Syst. Res. 52 (2018) 36–48. https://doi.org/https://doi.org/10.1016/j.cogsys.2018.06.006.

[19] W. Poewe, K. Seppi, C.M. Tanner, G.M. Halliday, P. Brundin, J. Volkmann, A.-E. Schrag, A.E. Lang, Parkinson disease, Nat. Rev. Dis. Prim. 3 (2017) 17013. https://doi.org/10.1038/nrdp.2017.13.

[20] R. Cools, Dopaminergic modulation of cognitive function-implications for L-DOPA treatment in Parkinson's disease, Neurosci. Biobehav. Rev. 30 (2006) 1–23. https://doi.org/10.1016/j.neubiorev.2005.03.024.

[21] M.H.R. Ludtmann, P.R. Angelova, M.H. Horrocks, M.L. Choi, M. Rodrigues, A.Y. Baev, A. V. Berezhnov, Z. Yao, D. Little, B. Banushi, A.S. Al-Menhali, R.T. Ranasinghe, D.R. Whiten, R. Yapom, K.S. Dolt, M.J. Devine, P. Gissen, T. Kunath, M. Jaganjac, E. V. Pavlov, D. Klenerman, A.Y. Abramov, S. Gandhi, α-synuclein oligomers interact with ATP synthase and open the permeability transition pore in Parkinson's disease, Nat. Commun. 9 (2018) 2293. https://doi.org/10.1038/s41467-018-04422-2.

[22] S. Shishodia, Molecular mechanisms of curcumin action: Gene expression, BioFactors. 39 (2013) 37–55. https://doi.org/10.1002/biof.1041.

[23] F.S. Aldawsari, R.P. Aguiar, L.A.M. Wiirzler, R. Aguayo-Ortiz, N. Aljuhani, R.K.N. Cuman, J.L. Medina-Franco, A.G. Siraki, C.A. Velázquez-Martínez, Anti-inflammatory and antioxidant properties of a novel resveratrol-salicylate hybrid analog, Bioorganic Med. Chem. Lett. 26 (2016) 1411–1415. https://doi.org/10.1016/j.bmcl.2016.01.069.

[24] M. de Freitas Silva, K.S.T. Dias, V.S. Gontijo, C.J.C. Ortiz, C. Viega, Multi-Target Directed Drugs as a Modern Approach for Drug Design Towards Alzheimer's Disease: an update, Curr. Med. Chem. 25 (2018). https://doi.org/10.2174/0929867325666180111101843.

[25] X. Chen, M. Decker, Multi-Target Compounds Acting in the Central Nervous System Designed From Natural Products, Curr. Med. Chem. 20 (2013) 1673–1685. https://doi.org/10.2174/0929867311320130007.

[26] C. Angeloni, D. Vauzour, Natural Products and Neuroprotection, Int. J. Mol. Sci. 20 (2019) 5570. https://doi.org/10.3390/ijms20225570.

[27] D.J. Newman, G.M. Cragg, Natural Products as Sources of New Drugs over the Nearly Four Decades from 01/1981 to 09/2019, J. Nat. Prod. 83 (2020) 770–803. https://doi.org/10.1021/acs.jnatprod.9b01285.

[28] C.J. Viegas, A. Danuello, V.S. Bolzani, E.J. Barreiro, C.M. Fraga, Molecular Hybridization: A Useful Tool in the Design of New Drug Prototypes, Curr. Med. Chem. 14 (2007) 1829–1852.

https://doi.org/10.2174/092986707781058805.

[29] V.S. Gontijo, F.P.D. Viegas, C.J.C. Ortiz, M. de Freitas Silva, C.M. Damasio, M.C. Rosa, T.G. Campos, D.S. Couto, K.S. Tranches Dias, C. Viegas, Molecular Hybridization as a Tool in the Design of Multi-target Directed Drug Candidates for Neurodegenerative Diseases, Curr. Neuropharmacol. 18 (2020) 348–407. https://doi.org/10.2174/1385272823666191021124443.

[30] M. Singh, M. Kaur, N. Chadha, O. Silakari, Hybrids: a new paradigm to treat Alzheimer's disease, Mol. Divers. 20 (2016) 271–297. https://doi.org/10.1007/s11030-015-9628-9.

[31] S.A. Carvalho, L.O. Feitosa, M. Soares, T.E.M.M. Costa, M.G. Henriques, K. Salomão, S.L. De Castro, M. Kaiser, R. Brun, J.L. Wardell, S.M.S.V. Wardell, G.H.G. Trossini, A.D. Andricopulo, E.F. Da Silva, C.A.M. Fraga, Design and synthesis of new (E)-cinnamic N-acylhydrazones as potent antitrypanosomal agents, Eur. J. Med. Chem. 54 (2012) 512–521. https://doi.org/10.1016/j.ejmech.2012.05.041.

[32] G. Palla, G. Predieri, P. Domiano, C. Vignali, W. Turner, Conformational behaviour and E/Z isomerization of N-acyl and N-aroylhydrazones, Tetrahedron. 42 (1986) 3649–3654. https://doi.org/10.1016/S0040-4020(01)87332-4.

[33] T. Mosmann, Rapid colorimetric assay for cellular growth and survival: Application to proliferation and cytotoxicity assays, J. Immunol. Methods. 65 (1983) 55–63. https://doi.org/10.1016/0022-1759(83)90303-4.

[34] N.C. Ammerman, M. Beier-Sexton, A.F. Azad, Growth and Maintenance of Vero Cell Lines, Curr. Protoc. Microbiol. 11 (2008). https://doi.org/10.1002/9780471729259.mca04es11.

[35] S. Rourou, M. Ben Zakkour, H. Kallel, Adaptation of Vero cells to suspension growth for rabies virus production in different serum free media, Vaccine. 37 (2019) 6987–6995. https://doi.org/10.1016/j.vaccine.2019.05.092.

[36] K.S.T. Dias, C.T. de Paula, T. dos Santos, I.N.O. Souza, M.S. Boni, M.J.R. Guimarï¿½es, F.M.R. da Silva, N.G. Castro, G.A. Neves, C.C. Veloso, M.M. Coelho, I.S.F. de Melo, F.C.V. Giusti, A. Giusti-Paiva, M.L. da Silva, L.E. Dardenne, I.A. Guedes, L. Pruccoli, F. Morroni, A. Tarozzi, C. Viegas, Design, synthesis and evaluation of novel feruloyl-donepezil hybrids as potential multitarget drugs for the treatment of Alzheimer's disease, Eur. J. Med. Chem. 130 (2017) 440–457. https://doi.org/10.1016/j.ejmech.2017.02.043.

[37] K. Jomova, D. Vondrakova, M. Lawson, M. Valko, Metals, oxidative stress and neurodegenerative disorders, Mol. Cell. Biochem. 345 (2010) 91–104. https://doi.org/10.1007/s11010-010-0563-x.

[38] L. Baum, A. Ng, Curcumin interaction with copper and iron suggests one possible mechanism of action in Alzheimer ' s disease animal models, J. Alzheimer's Dis. 6 (2004) 367–377.

https://doi.org/10.3233/JAD-2004-6403.

[39] M.L. Bolognesi, A. Cavalli, L. Valgimigli, M. Bartolini, M. Rosini, V. Andrisano, M. Recanatini, C. Melchiorre, Multi-Target-Directed Drug Design Strategy : From a Dual Binding Site Acetylcholinesterase Inhibitor to a Trifunctional Compound against Alzheimer ' s Disease Multi-Target-Directed Drug Design Strategy : From a Dual Binding Site Acetylcholinesterase Inhib, J. Med. Chem. 6 (2007) 6446–6449. https://doi.org/10.1021/jm701225u.

[40] M. Rullo, G. La Spada, D.V. Miniero, A. Gottinger, M. Catto, P. Delre, M. Mastromarino, T. Latronico, S. Marchese, G.F. Mangiatordi, C. Binda, A. Linusson, G.M. Liuzzi, L. Pisani, Bioisosteric replacement based on 1,2,4-oxadiazoles in the discovery of 1H-indazole-bearing neuroprotective MAO B inhibitors, Eur. J. Med. Chem. 255 (2023) 115352. https://doi.org/10.1016/j.ejmech.2023.115352.

[41] R.M.C. Di Martino, L. Pruccoli, A. Bisi, S. Gobbi, A. Rampa, A. Martinez, C. Pérez, L. Martinez-Gonzalez, M. Paglione, E. Di Schiavi, F. Seghetti, A. Tarozzi, F. Belluti, Novel Curcumin-Diethyl Fumarate Hybrid as a Dualistic GSK-3β Inhibitor/Nrf2 Inducer for the Treatment of Parkinson's Disease, ACS Chem. Neurosci. 11 (2020) 2728–2740. https://doi.org/10.1021/acschemneuro.0c00363.

[42] N.P. Rocha, A.S. de Miranda, A.L. Teixeira, Insights into Neuroinflammation in Parkinson's Disease: From Biomarkers to Anti-Inflammatory Based Therapies, Biomed Res. Int. 2015 (2015) 1–12. https://doi.org/10.1155/2015/628192.

[43] M.G. Tansey, R.L. Wallings, M.C. Houser, M.K. Herrick, C.E. Keating, V. Joers, Inflammation and immune dysfunction in Parkinson disease, Nat. Rev. Immunol. 22 (2022) 657–673. https://doi.org/10.1038/s41577-022-00684-6.

[44] P. Deshmukh, S. Unni, G. Krishnappa, B. Padmanabhan, The Keap1–Nrf2 pathway: promising therapeutic target to counteract ROS-mediated damage in cancers and neurodegenerative diseases, Biophys. Rev. 9 (2017) 41–56. https://doi.org/10.1007/s12551-016-0244-4.

[45] S. Dayalan Naidu, A.T. Dinkova-Kostova, KEAP1, a cysteine-based sensor and a drug target for the prevention and treatment of chronic disease, Open Biol. 10 (2020). https://doi.org/10.1098/rsob.200105.

[46] A. Cleasby, J. Yon, P.J. Day, C. Richardson, I.J. Tickle, P.A. Williams, J.F. Callahan, R. Carr, N. Concha, J.K. Kerns, H. Qi, T. Sweitzer, P. Ward, T.G. Davies, Structure of the BTB domain of Keap1 and its interaction with the triterpenoid antagonist CDDO, PLoS One. 9 (2014). https://doi.org/10.1371/journal.pone.0098896.

[47] C. Huerta, X. Jiang, I. Trevino, C.F. Bender, D.A. Ferguson, B. Probst, K.K. Swinger, V.S. Stoll, P.J. Thomas, I. Dulubova, M. Visnick, W.C. Wigley, Characterization of novel small-

molecule NRF2 activators: Structural and biochemical validation of stereospecific KEAP1 binding, Biochim. Biophys. Acta - Gen. Subj. 1860 (2016) 2537–2552. https://doi.org/10.1016/j.bbagen.2016.07.026.

[48] A. Pinto, Z. El Ali, S. Moniot, L. Tamborini, C. Steegborn, R. Foresti, C. De Micheli, Effects of 3-Bromo-4,5-dihydroisoxazole Derivatives on Nrf2 Activation and Heme Oxygenase-1 Expression, ChemistryOpen. 7 (2018) 858–864. https://doi.org/10.1002/open.201800185.

[49] T. Ohnuma, S. Nakayama, E. Anan, T. Nishiyama, K. Ogura, A. Hiratsuka, Activation of the Nrf2/ARE pathway via S-alkylation of cysteine 151 in the chemopreventive agent-sensor Keap1 protein by falcarindiol, a conjugated diacetylene compound, Toxicol. Appl. Pharmacol. 244 (2010) 27–36. https://doi.org/10.1016/j.taap.2009.12.012.

[50] D.D. Perrim, W.L.F. Armarengo, Purification of Laboratory Chemicals, 3rd ed., Pergamon Press, 1988.

[51] V.S. Gontijo, T.C. De Souza, I.A. Rosa, M.G. Soares, M.A. Da Silva, W. Vilegas, C. Viegas, M.H. Dos Santos, Isolation and evaluation of the antioxidant activity of phenolic constituents of the Garcinia brasiliensis epicarp, Food Chem. 132 (2012) 1230–1235. https://doi.org/10.1016/j.foodchem.2011.10.110.

[52] S.-Y. Chen, Y. Chen, Y.-P. Li, S.-H. Chen, J.-H. Tan, T.-M. Ou, L.-Q. Gu, Z.-S. Huang, Design, synthesis, and biological evaluation of curcumin analogues as multifunctional agents for the treatment of Alzheimer's disease, Bioorg. Med. Chem. 19 (2011) 5596–5604. https://doi.org/10.1016/j.bmc.2011.07.033.

[53] M. Guardigni, L. Pruccoli, A. Santini, A. De Simone, M. Bersani, F. Spyrakis, F. Frabetti, E. Uliassi, V. Andrisano, B. Pagliarani, P. Fernández-Gómez, V. Palomo, M.L. Bolognesi, A. Tarozzi, A. Milelli, PROTAC-Induced Glycogen Synthase Kinase 3β Degradation as a Potential Therapeutic Strategy for Alzheimer's Disease, ACS Chem. Neurosci. 14 (2023) 1963–1970. https://doi.org/10.1021/acschemneuro.3c00096.

[54] C.J.C. Ortiz, C.M. Damasio, L. Pruccoli, N.F. Nadur, L.L. de Azevedo, I.A. Guedes, L.E. Dardenne, A.E. Kümmerle, A. Tarozzi, C. Viegas, Cinnamoyl-N-Acylhydrazone-Donepezil Hybrids: Synthesis and Evaluation of Novel Multifunctional Ligands Against Neurodegenerative Diseases, Neurochem. Res. 45 (2020) 3003–3020. https://doi.org/10.1007/s11064-020-03148-2.

[55] E. De Lorenzi, F. Seghetti, A. Tarozzi, L. Pruccoli, C. Contardi, M. Serra, A. Bisi, S. Gobbi, G. Vistoli, S. Gervasoni, C. Argentini, G. Ghirardo, G. Guarato, G. Orso, F. Belluti, R.M.C. Di Martino, M. Zusso, Targeting the multifaceted neurotoxicity of Alzheimer's disease by tailored functionalisation of the curcumin scaffold, Eur. J. Med. Chem. 252 (2023) 115297.

https://doi.org/10.1016/j.ejmech.2023.115297.

[56] H.M. Campos, M. da Costa, L.K. da Silva Moreira, H.F. da Silva Neri, C.R. Branco da Silva, L. Pruccoli, F.C.A. dos Santos, E.A. Costa, A. Tarozzi, P.C. Ghedini, Protective effects of chrysin against the neurotoxicity induced by aluminium: In vitro and in vivo studies, Toxicology. 465 (2022) 153033. https://doi.org/10.1016/j.tox.2021.153033.

[57] L. Pisani, R. Farina, M. Catto, R.M. Iacobazzi, O. Nicolotti, S. Cellamare, G.F. Mangiatordi, N. Denora, R. Soto-Otero, L. Siragusa, C.D. Altomare, A. Carotti, Exploring Basic Tail Modifications of Coumarin-Based Dual Acetylcholinesterase-Monoamine Oxidase B Inhibitors: Identification of Water-Soluble, Brain-Permeant Neuroprotective Multitarget Agents, J. Med. Chem. 59 (2016) 6791–6806. https://doi.org/10.1021/acs.jmedchem.6b00562.

Declaration of interests

The authors declare no conflict of interest related to the submitted manuscript titled "**Synthesis and Pharmacological Evaluation of Novel *N*-aryl-cinnamoyl-hydrazone Hybrids Designed as Neuroprotective Agents for the Treatment of Parkinson's Disease**".

Declaration of interests

☐The authors declare that they have no known competing financial interests or personal relationships that could have appeared to influence the work reported in this paper.

☒The authors declare the following financial interests/personal relationships which may be considered as potential competing interests:

Claudio Viegas Jr reports financial support, administrative support, and equipment, drugs, or supplies were provided by National Council for Scientific and Technological Development. Claudio Viegas Jr. reports financial support was provided by Minas Gerais State Foundation of Support to the Research. Claudio Viegas Jr reports financial support was provided by Federal University of Alfenas. If there are other authors, they declare that they have no known competing financial interests or personal relationships that could have appeared to influence the work reported in this paper.